Evaluating Hex-mesh Quality Metrics via Correlation Analysis
Supplemental material

I. Deviation Matrices

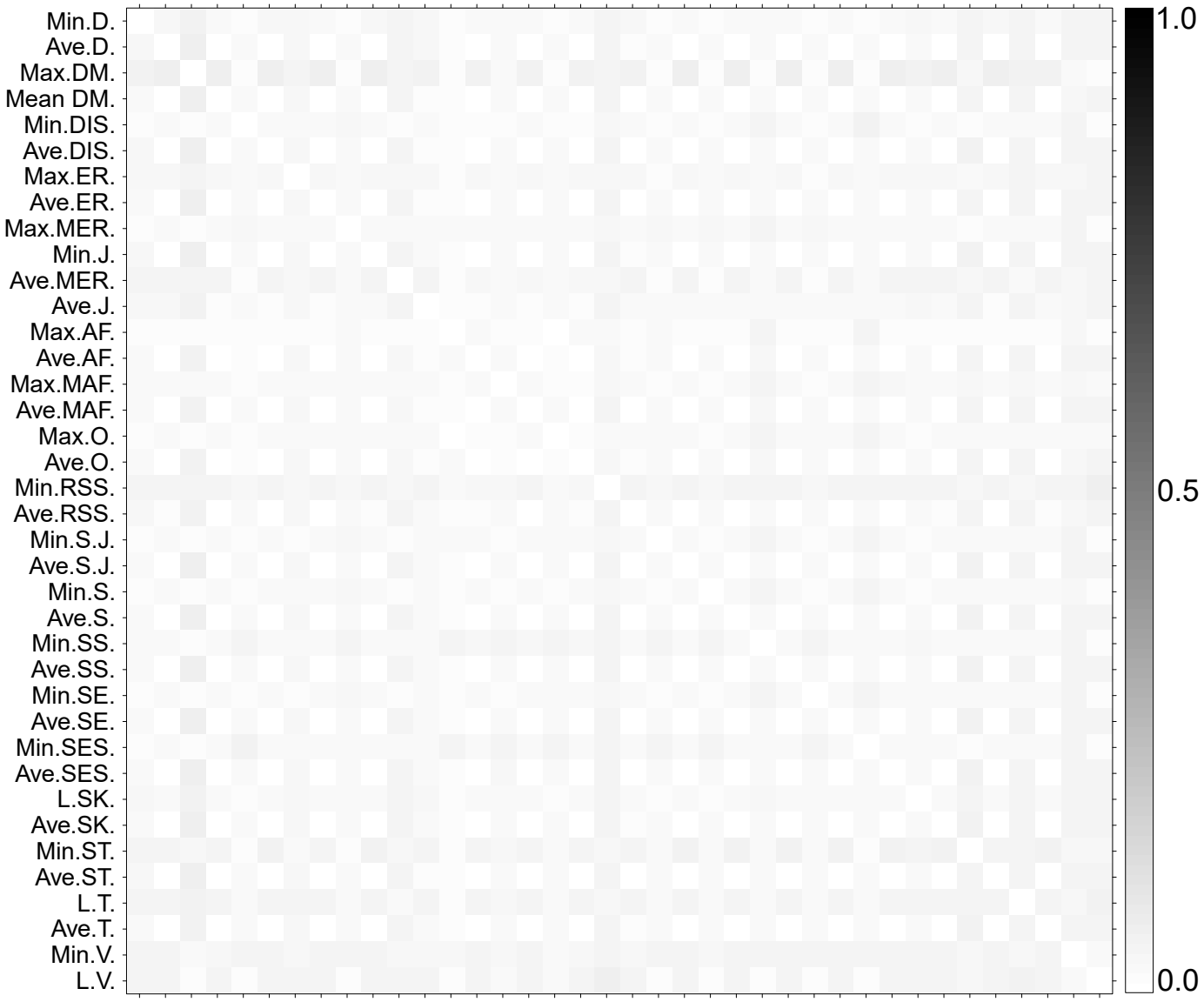

Fig. 1: Deviation matrix of the 22 datasets w.r.t. the averaged correlation matrix shown in Figure 3 of the paper.

II. Datasets and Correlation Matrices

This section provides the statistics and correlation analysis results for all the models used in our study. Specifically, Table I details the statistics of the individual datasets, including the number of meshes generated for each model in each level of the data generation and the times spent on the data generation and the computing of the involved systems for the three applications, respectively.

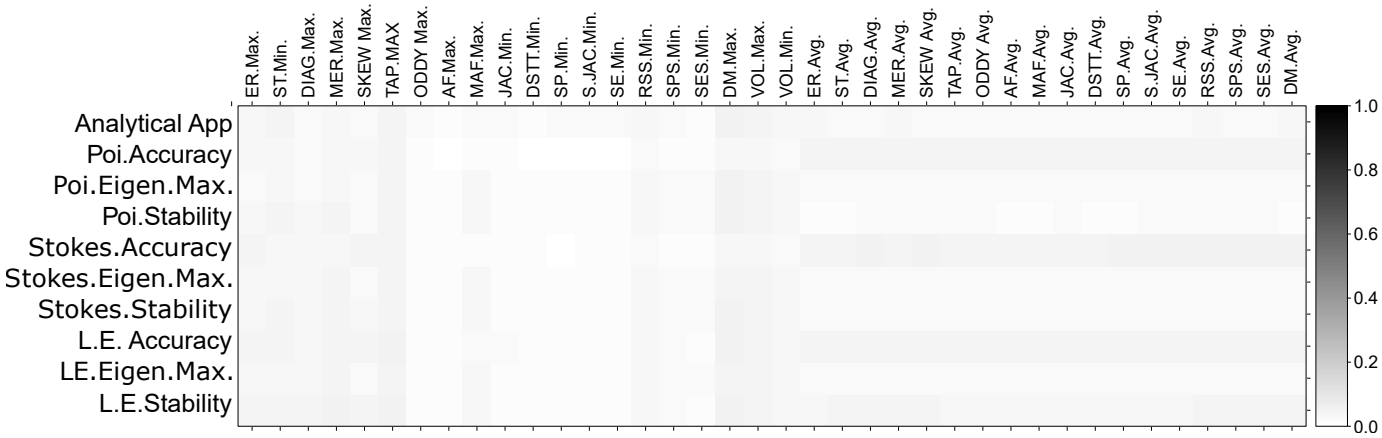

Fig. 2: Deviation matrix of the 22 datasets w.r.t. the averaged correlation matrix shown in Figure 6 of the paper.

TABLE I: Statistics of different datasets. #H shows the number of hexahedral elements of each mesh of a model. α and β are the parameters used in the two-level noise insertion data generation (see the paper for details). $\mathcal{H}_{Min}$ is the number of meshes generated via the control of the minimum metrics (i.e., the first level of data generation), while $\mathcal{H}_{Ave}$ shows the total number of generated hex-meshes for a model. $\mathcal{F}_{Ave}$ is the number of meshes we selected from $\mathcal{H}_{Ave}$ for the correlation study. G. Time provides the timing information of data generation. A. Time, P. Time, and S. Time are the times spent on computing the analytical solution, Poisson and Stokes simulations, respectively. The time spent on the computation of the linear elasticity problem is almost identical to the time on the Stokes simulation. Therefore, we do not report them here.

Models	#H	α	β	$\mathcal{H}_{Min}$	$\mathcal{H}_{Ave}$	$\mathcal{F}_{Ave}$	G. Time	A. Time	P. Time	S. time
anc101	8030	8	20	59	4777	714	54.0h	0.5h	0.8h	16.0h
angel_1	5600	8	20	60	4644	606	41.5h	0.3h	0.5h	8.0h
armadillo	9214	8	20	56	4177	721	57.5h	0.6h	0.8h	22.0h
bone	3396	8	20	64	3724	525	24.0h	0.2h	0.3h	4.0h
bust	5398	8	20	57	2752	607	40.0h	0.4h	0.5h	7.0h
bumpy_torus	8908	8	20	59	4601	639	60.0h	0.8h	0.5h	21.0h
bunny	4552	8	20	60	3903	735	34.0h	0.3h	0.5h	5.0h
canew	5515	8	20	56	4505	751	61.0h	0.3h	0.5h	8.0h
crank	10440	8	20	67	3822	818	64.0h	0.7h	1.0h	30.0h
dancingchildren	13192	8	20	61	4763	618	69.0h	0.8h	1.0h	30.0h
double_torus	3695	8	20	63	3016	633	20.0h	0.3h	0.5h	4.0h
elephant	8730	8	20	49	3795	643	51.0h	0.5h	0.8h	20.0h
gargoyle	13228	8	20	62	4806	616	73.0h	0.8h	1.0h	30.0h
fertility	8069	8	20	59	4031	817	55.0h	0.6h	0.8h	16.0h
hanger	4539	8	20	62	3634	719	25.5h	0.3h	0.5h	5.0h
impeller	5637	8	20	59	2930	619	29.0h	0.4h	0.5h	8.0h
joint	4755	8	20	62	2877	586	27.0h	0.4h	0.5h	5.0h
kiss	8315	8	20	54	4996	828	56.0h	0.6h	1.0h	18.0h
KingKong	5055	8	20	59	3668	548	36.5h	0.4h	0.5h	5.0h
kitty	5045	8	20	60	3736	692	35.0h	0.4h	0.5h	4.0h
rockerarm	5993	8	20	59	4554	565	61.0h	0.3h	0.5h	9.0h
rod	4746	8	20	61	2940	786	35.0h	0.4h	0.5h	6.0h

The following figures provide the visualization of the correlation analysis results (i.e., the full correlation matrix of each model) and the parallel coordinate visualizations of the distribution of the sampled meshes for each model in the metric space. These parallel coordinate visualizations demonstrate that the metric values of the selected meshes for study are still well-distributed in the metric space.

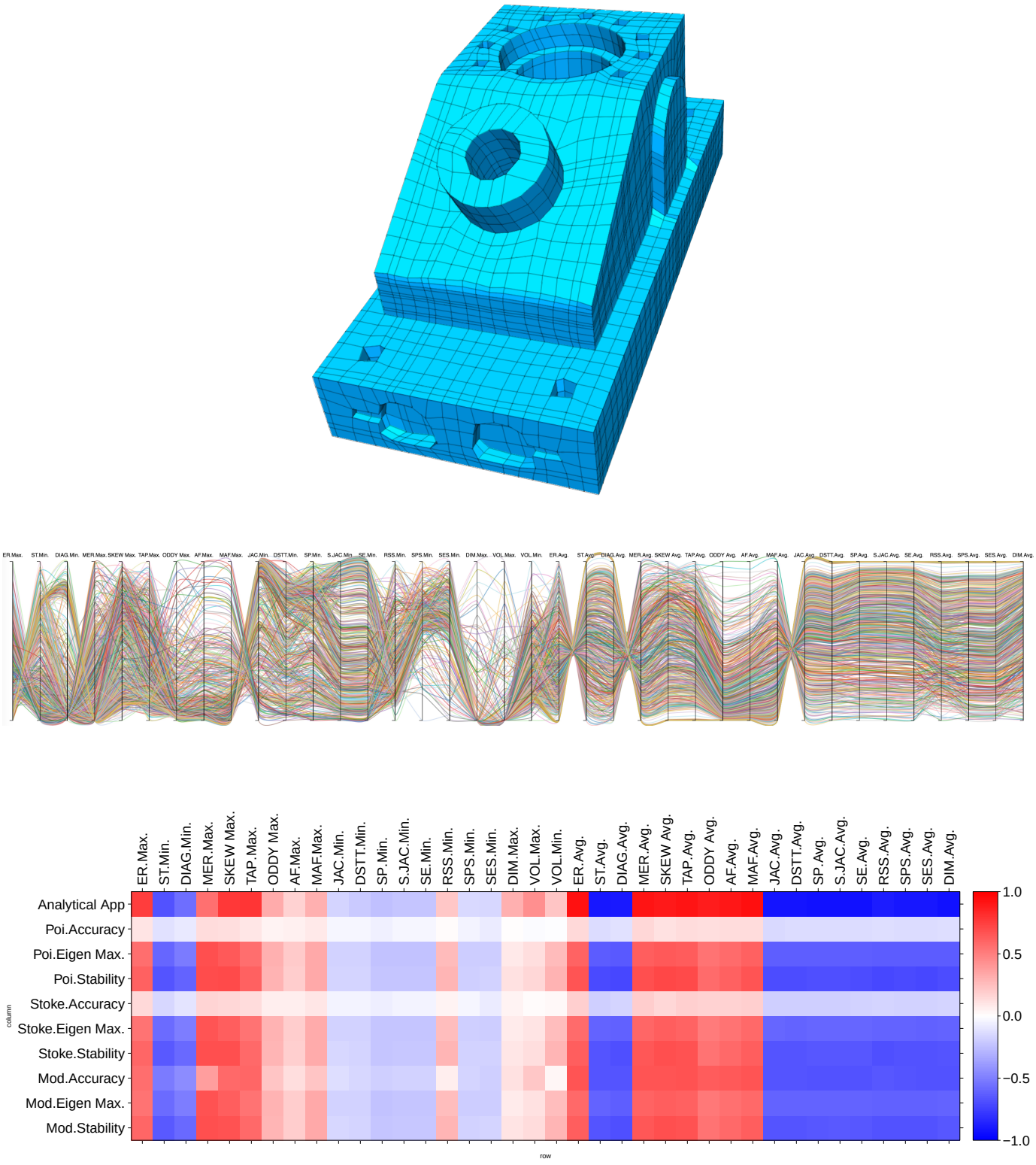

Fig. 3: The anc101 model (top), the parallel coordinate visualization of the sampled meshes (714 in total) in the metric space (middle), and the correlation matrix of the 38 metrics versus the Accuracy, Stability, and the difference of the solved maximal eigenvalue from the ground-truth (i.e., Max.Eigen) for the three simulations and the analytical application (bottom).

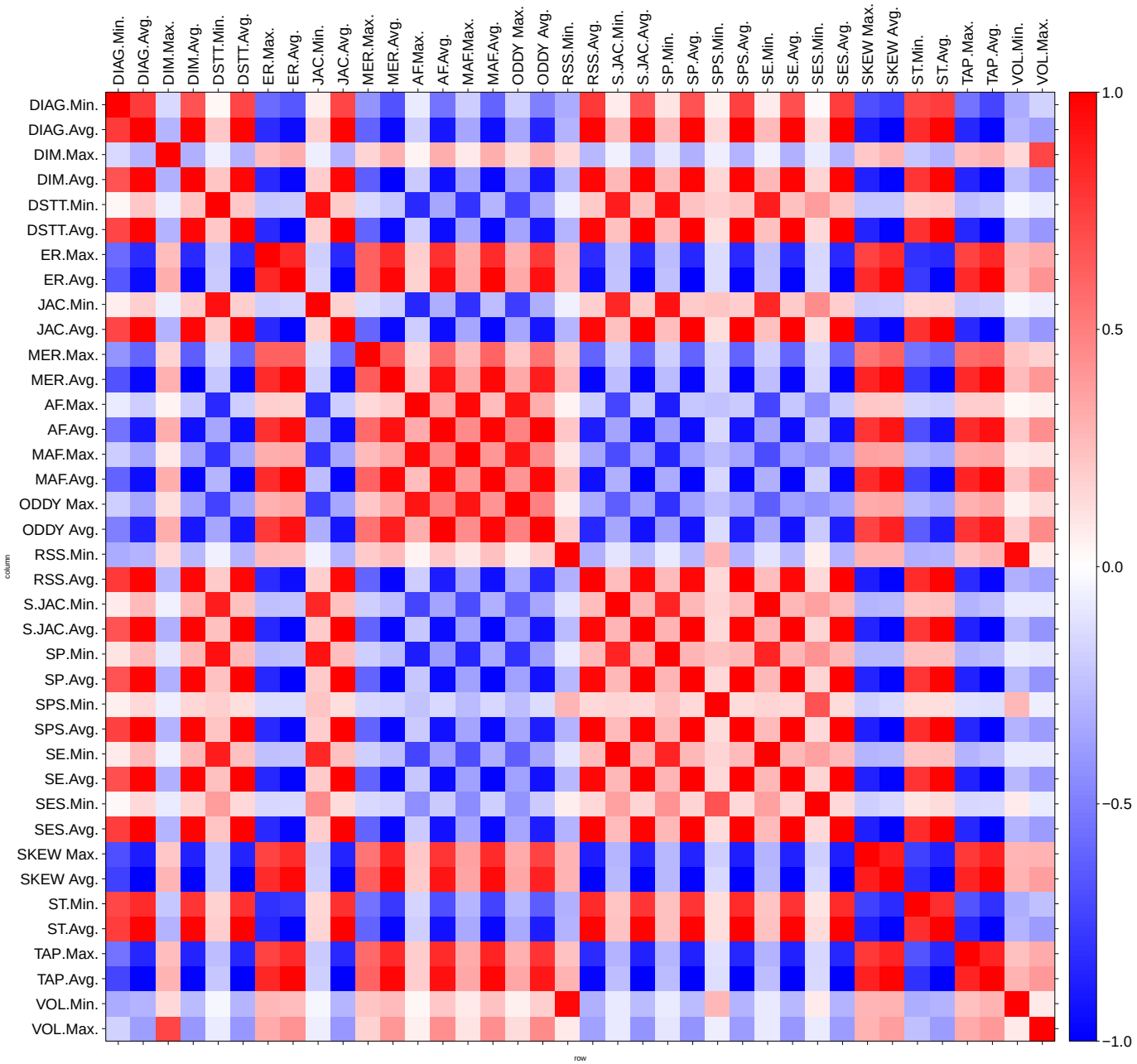

Fig. 4: The correlation matrix of the 38 metrics for the anc101 model.

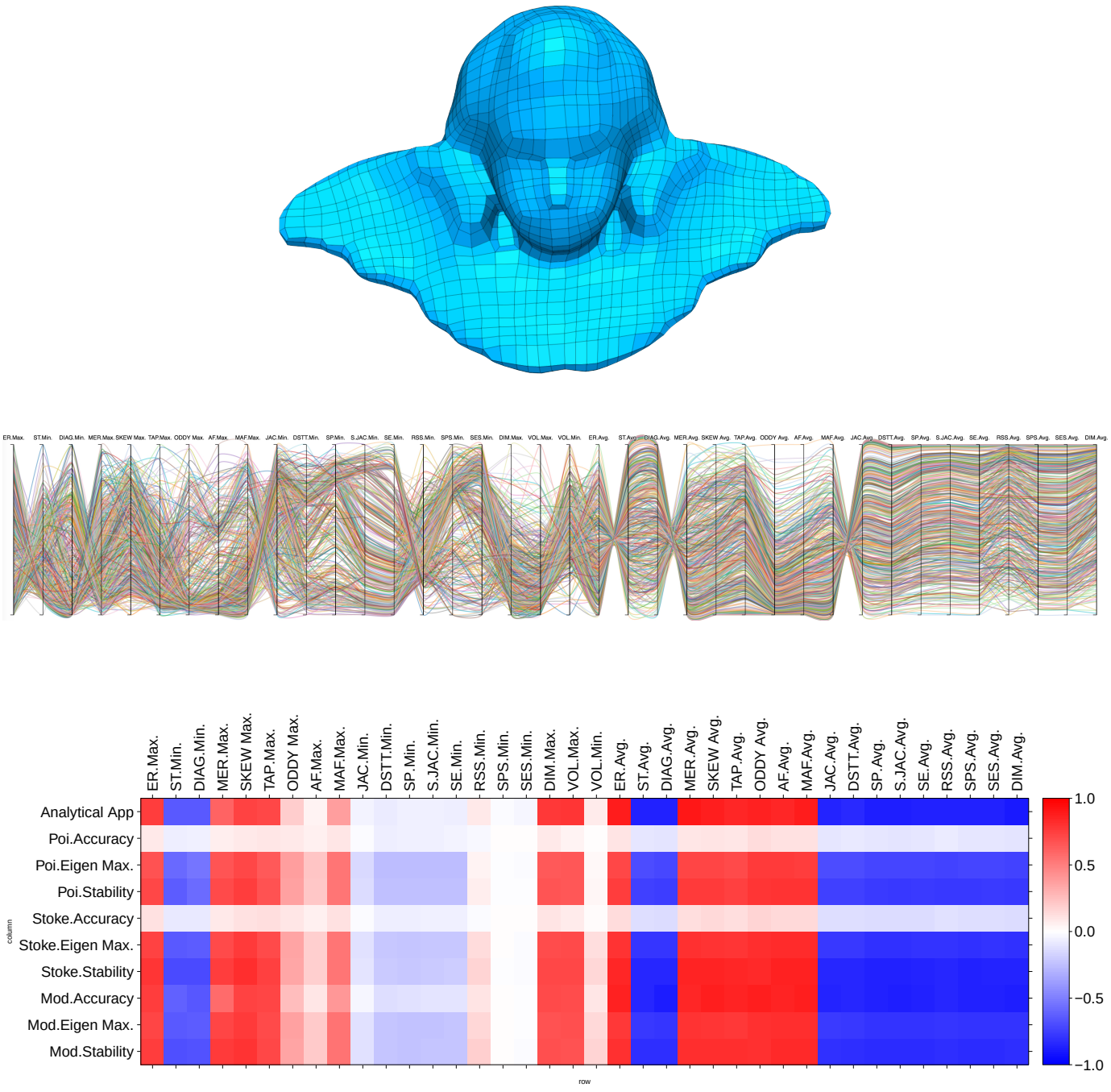

Fig. 5: The angel model (top), the parallel coordinate visualization of the sampled meshes (606 in total) in the metric space (middle), and the correlation matrix of the 38 metrics versus the Accuracy, Stability, and the difference of the solved maximal eigenvalue from the ground-truth (i.e., Max.Eigen) for the three simulations and the analytical application (bottom).

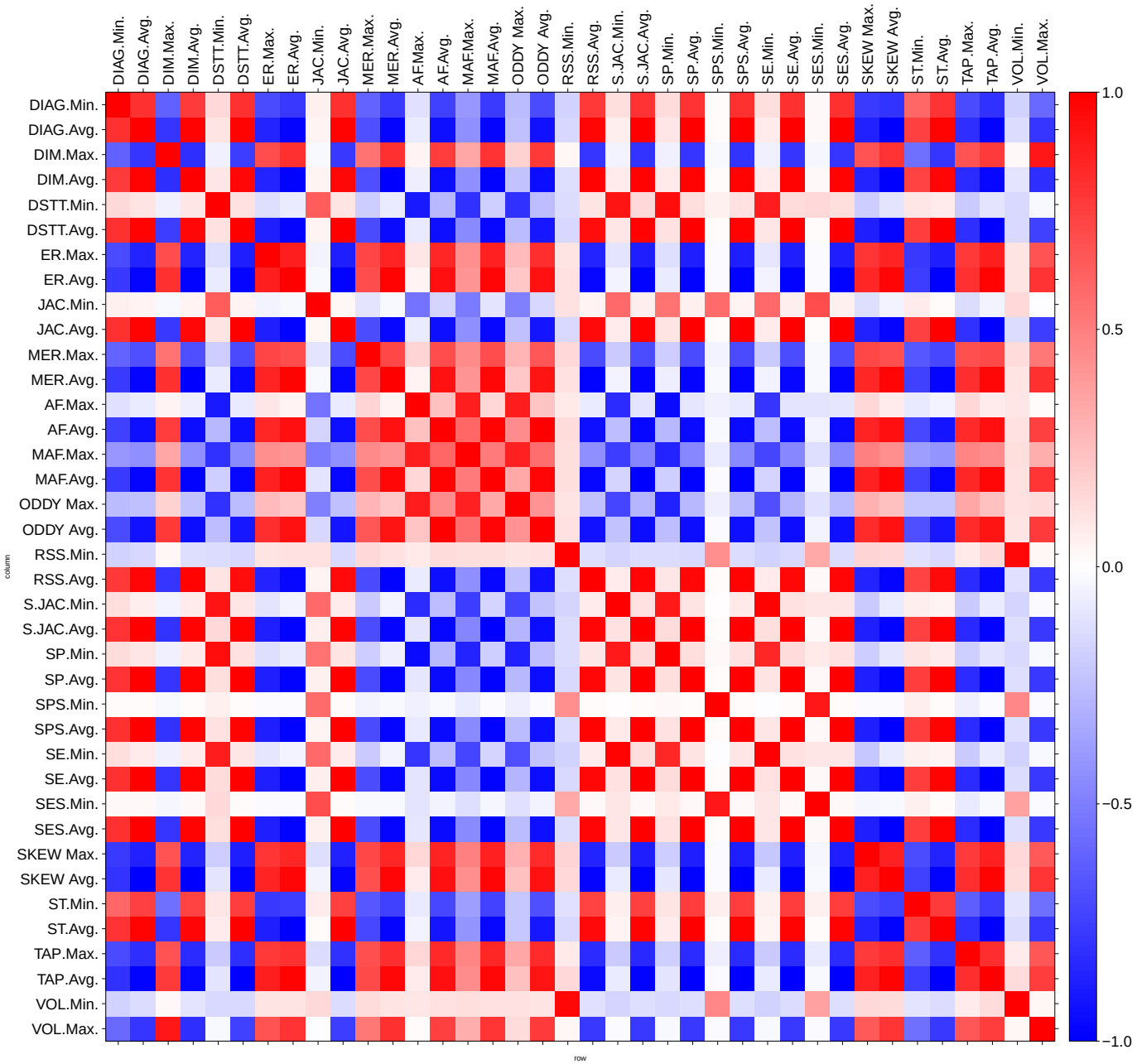

Fig. 6: The correlation matrix of the 38 metrics for the angel model.

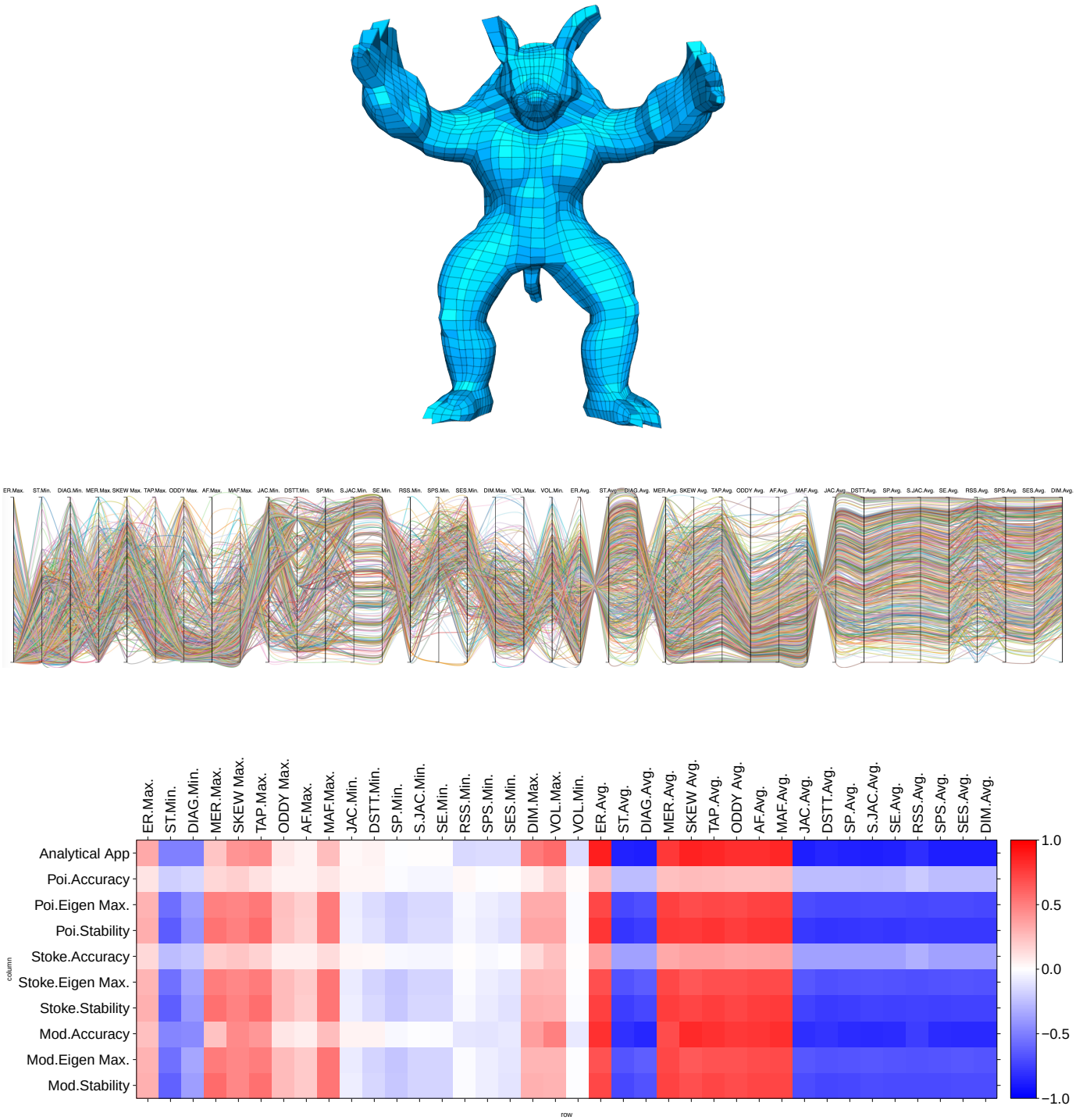

Fig. 7: The armadillo model (top), the parallel coordinate visualization of the sampled meshes (721 in total) in the metric space (middle), and the correlation matrix of the 38 metrics versus the Accuracy, Stability, and the difference of the solved maximal eigenvalue from the ground-truth (i.e., Max.Eigen) for the three simulations and the analytical application (bottom).

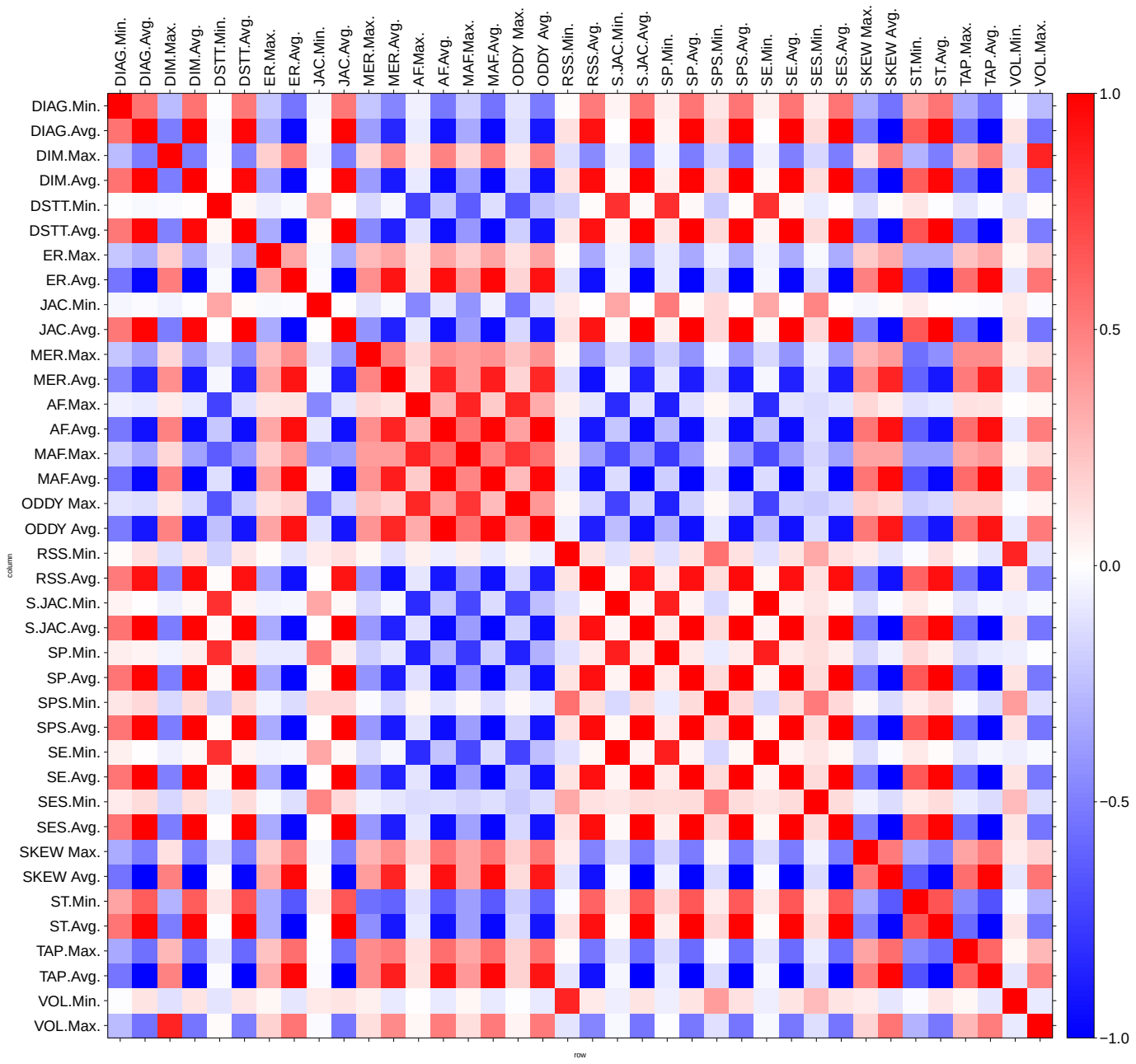

Fig. 8: The armadillo correlation matrix of the 38 metrics for the model.

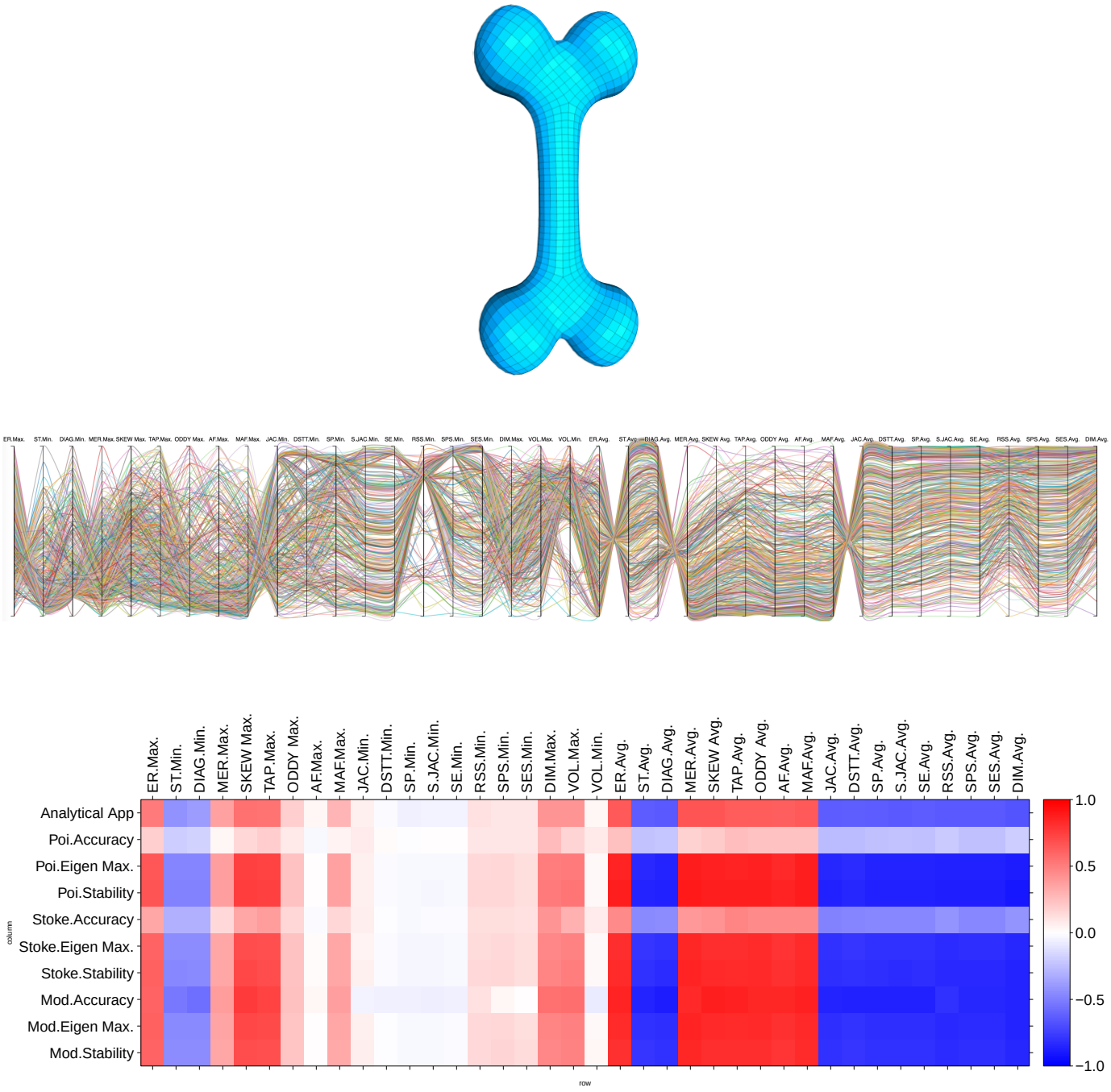

Fig. 9: The bone model (top), the parallel coordinate visualization of the sampled meshes (525 in total) in the metric space (middle), and the correlation matrix of the 38 metrics versus the Accuracy, Stability, and the difference of the solved maximal eigenvalue from the ground-truth (i.e., Max.Eigen) for the three simulations and the analytical application (bottom).

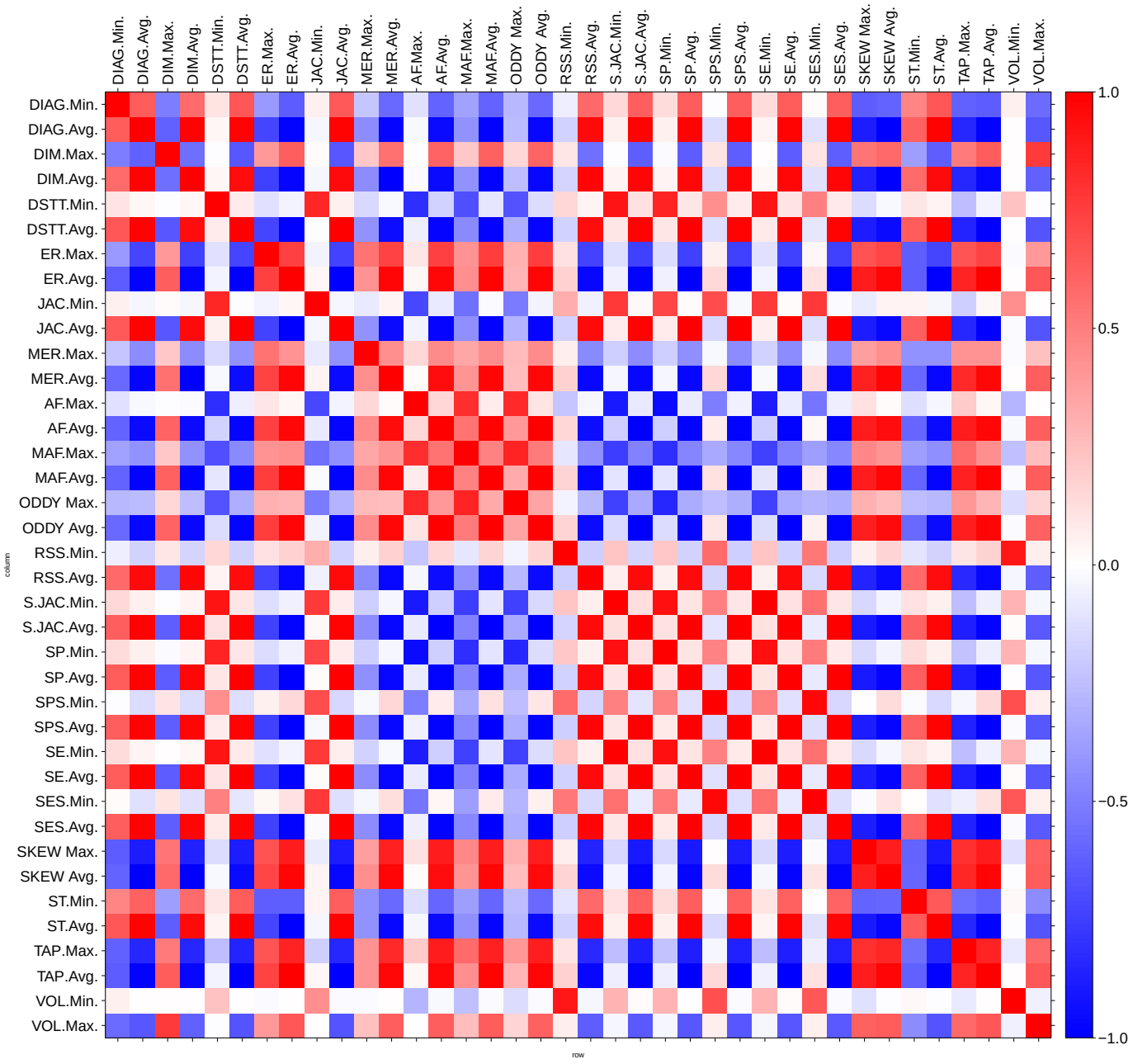

Fig. 10: The bone correlation matrix of the 38 metrics for the model.

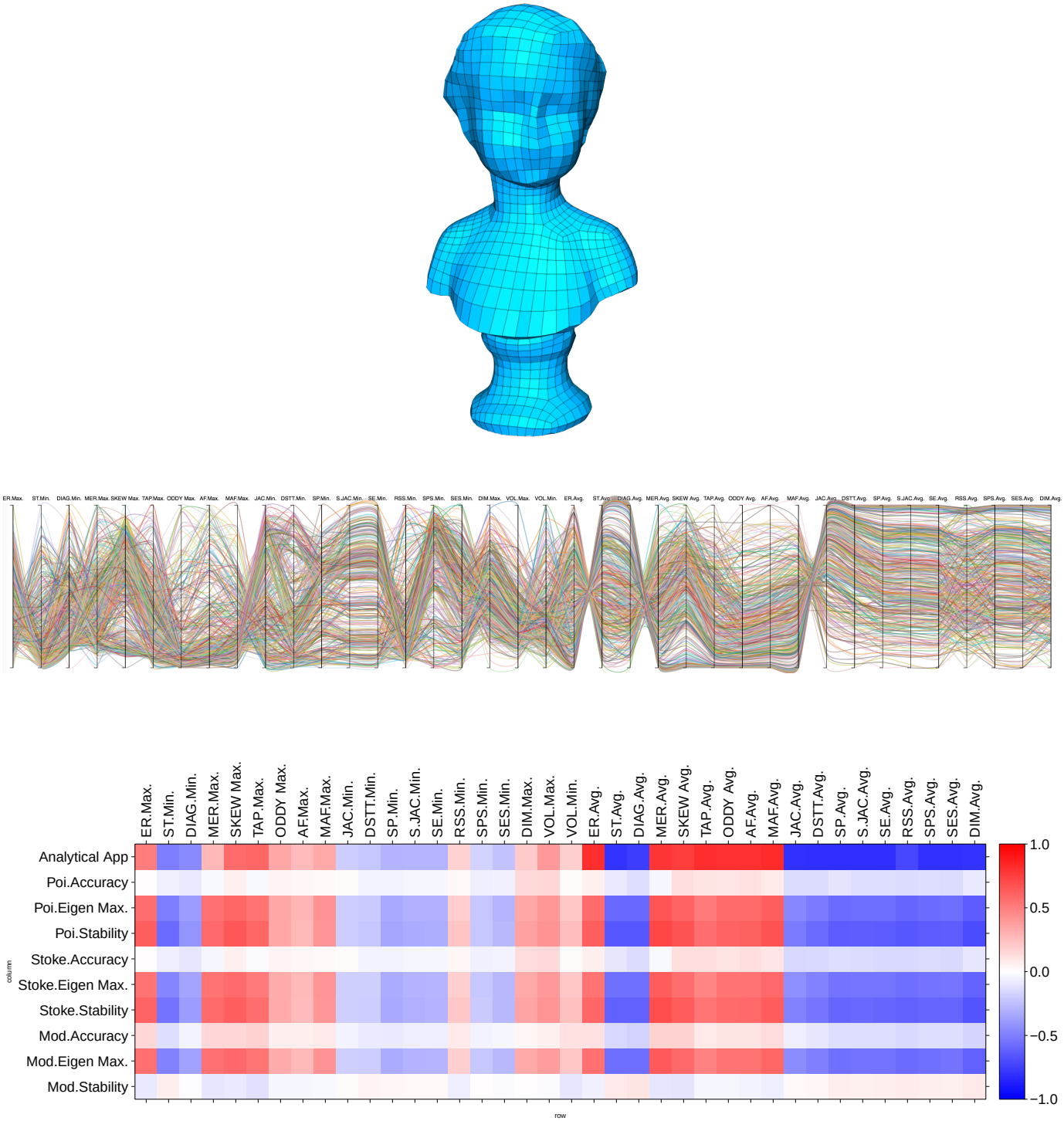

Fig. 11: The bust model (top), the parallel coordinate visualization of the sampled meshes (607 in total) in the metric space (middle), and the correlation matrix of the 38 metrics versus the Accuracy, Stability, and the difference of the solved maximal eigenvalue from the ground-truth (i.e., Max.Eigen) for the three simulations and the analytical application (bottom).

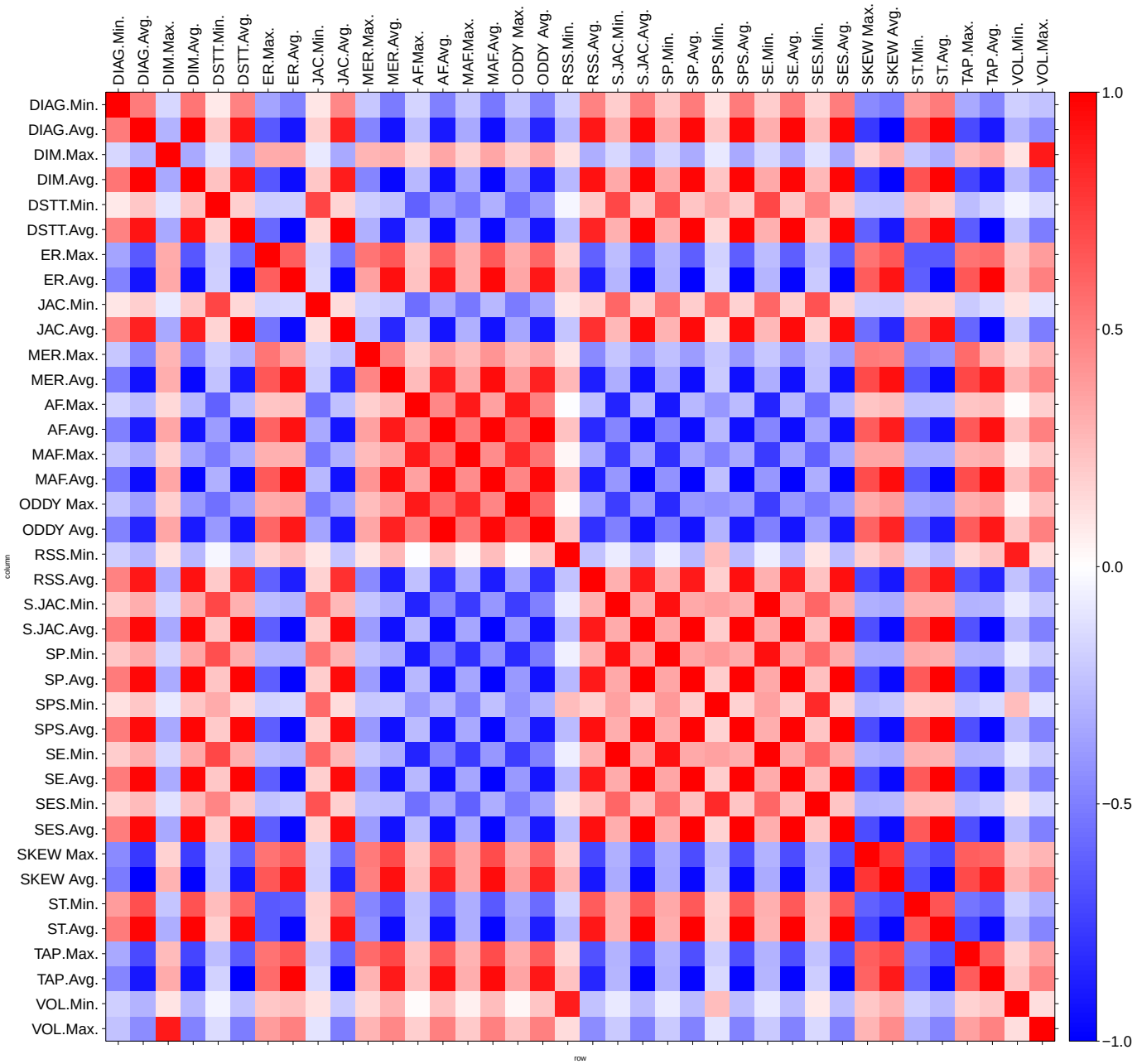

Fig. 12: The bust correlation matrix of the 38 metrics for the model.

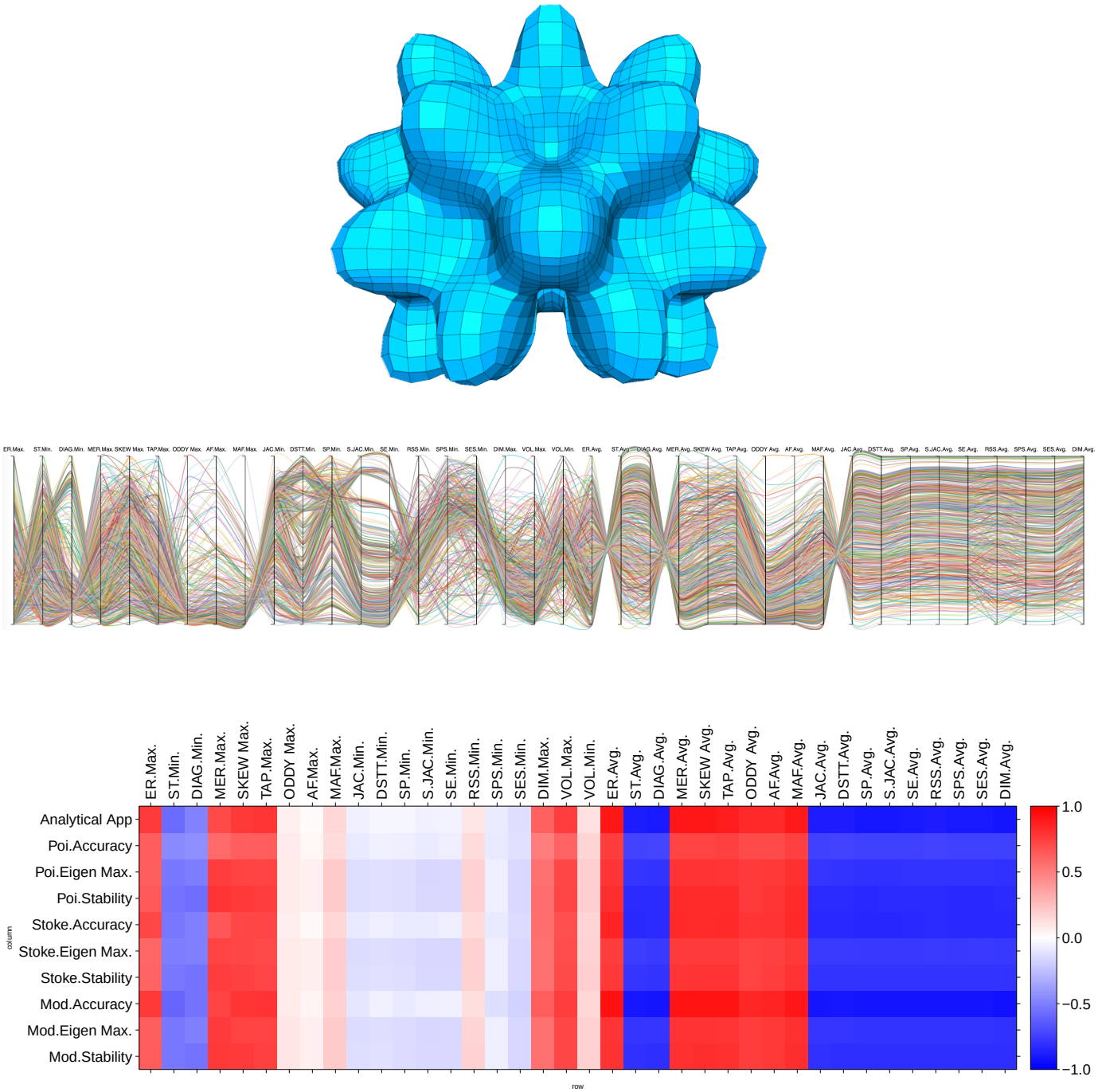

Fig. 13: The bumpy torus model (top), the parallel coordinate visualization of the sampled meshes (639 in total) in the metric space (middle), and the correlation matrix of the 38 metrics versus the Accuracy, Stability, and the difference of the solved maximal eigenvalue from the ground-truth (i.e., Max.Eigen) for the three simulations and the analytical application (bottom).

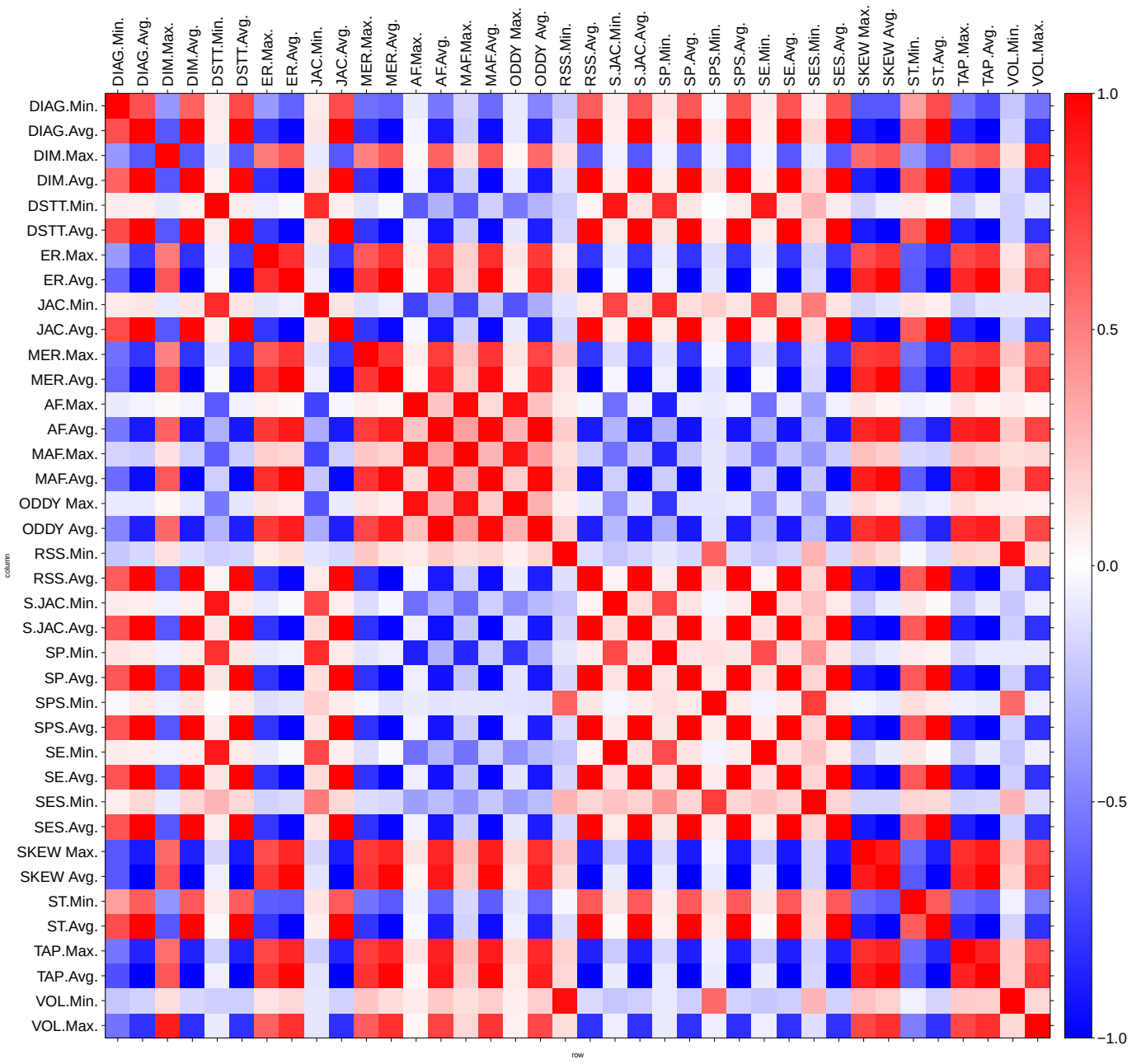

Fig. 14: The correlation matrix of the 38 metrics for the bumpy torus model.

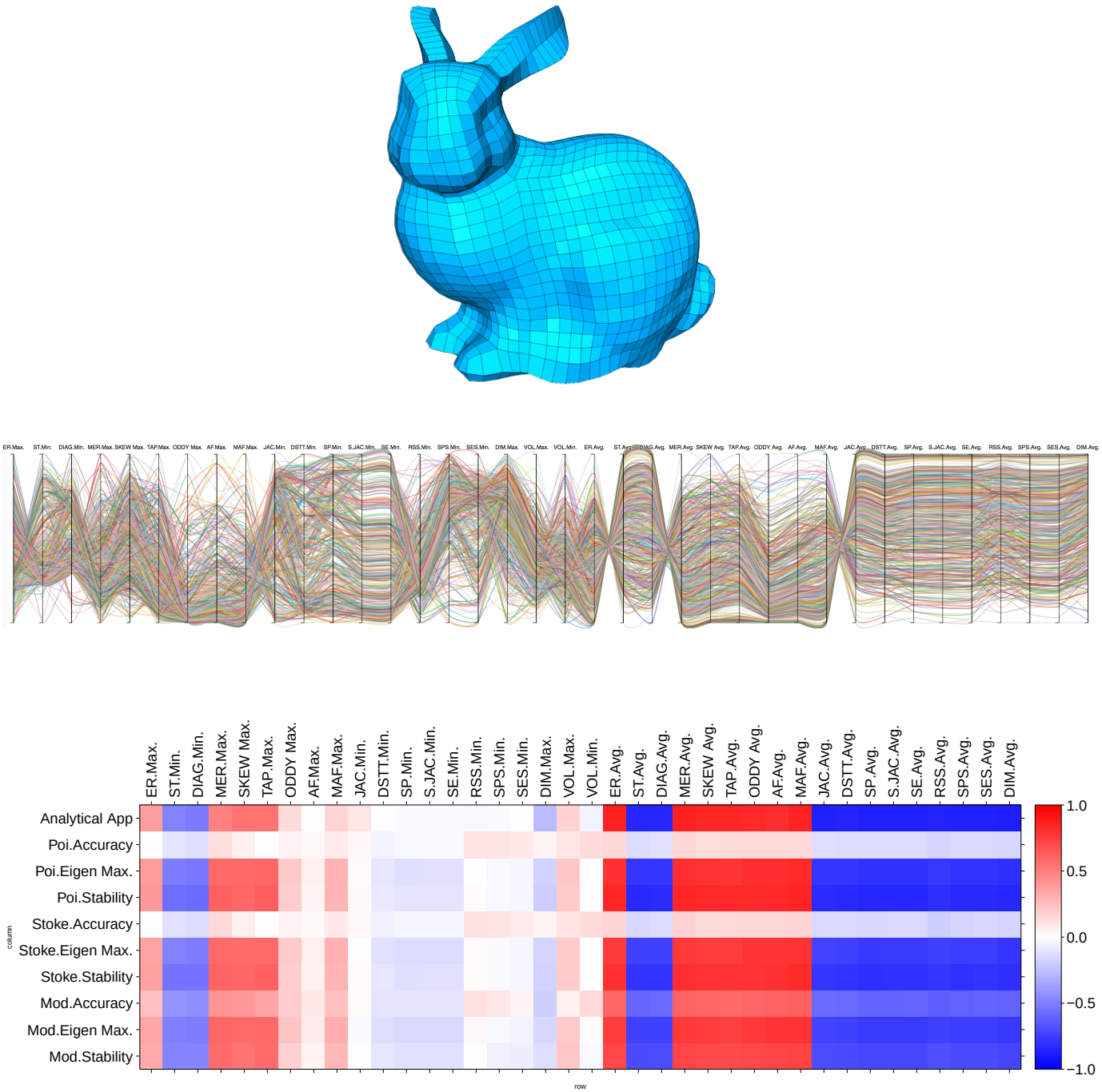

Fig. 15: The bunny model (top), the parallel coordinate visualization of the sampled meshes (735 in total) in the metric space (middle), and the correlation matrix of the 38 metrics versus the Accuracy, Stability, and the difference of the solved maximal eigenvalue from the ground-truth (i.e., Max.Eigen) for the three simulations and the analytical application (bottom).

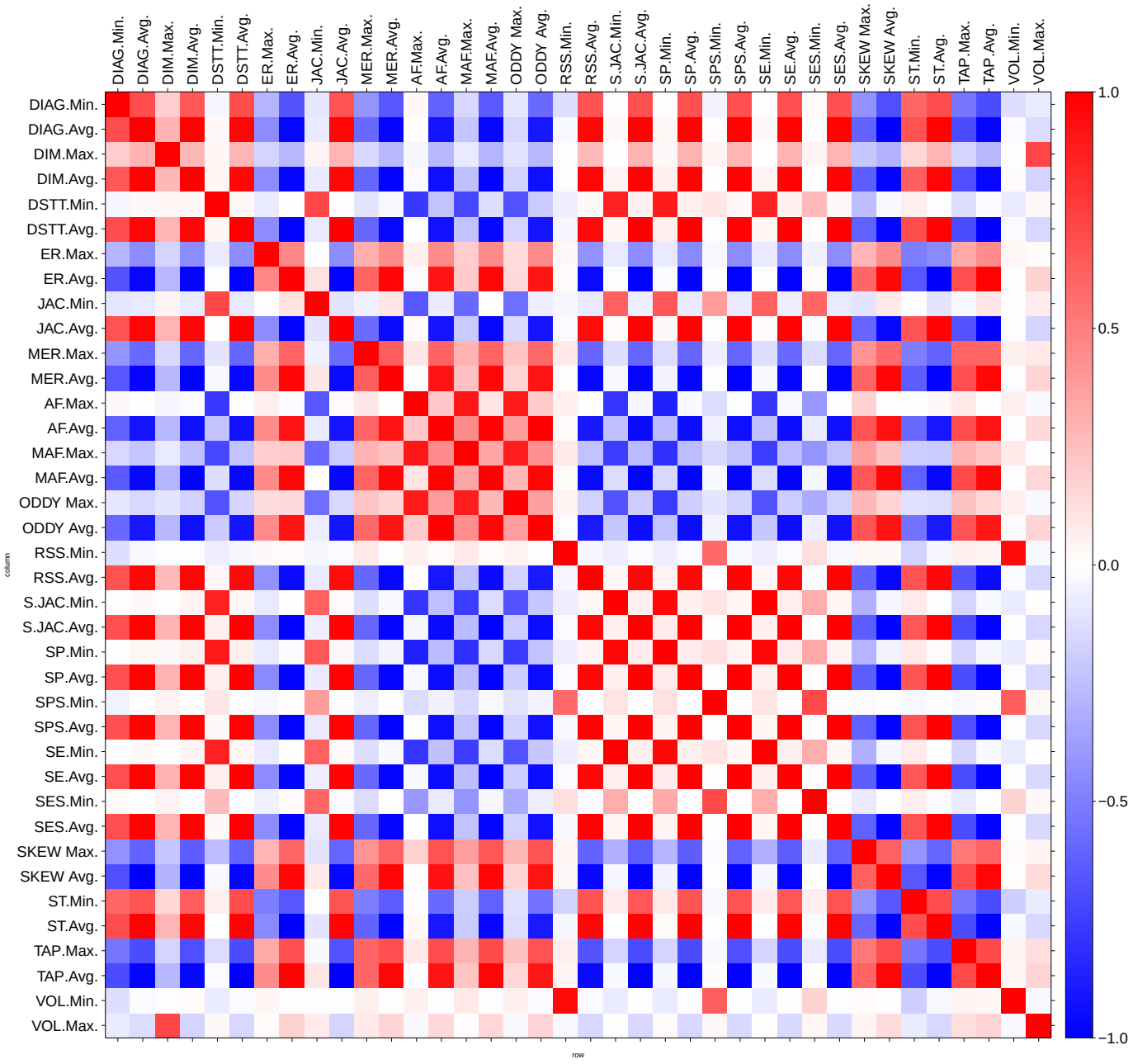

Fig. 16: The correlation matrix of the 38 metrics for the bunny model.

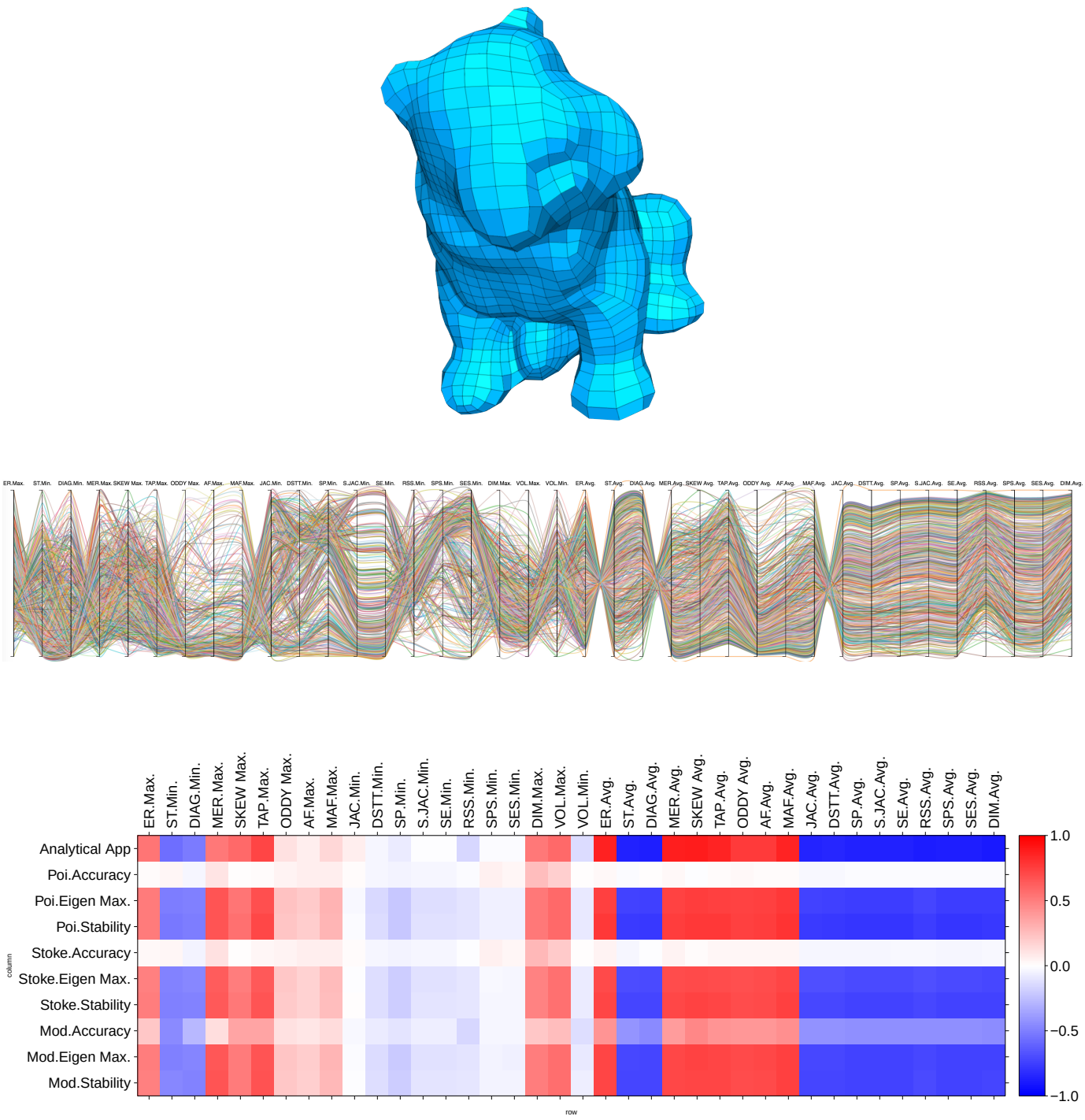

Fig. 17: The canew model (top), the parallel coordinate visualization of the sampled meshes (751 in total) in the metric space (middle), and the correlation matrix of the 38 metrics versus the Accuracy, Stability, and the difference of the solved maximal eigenvalue from the ground-truth (i.e., Max.Eigen) for the three simulations and the analytical application (bottom).

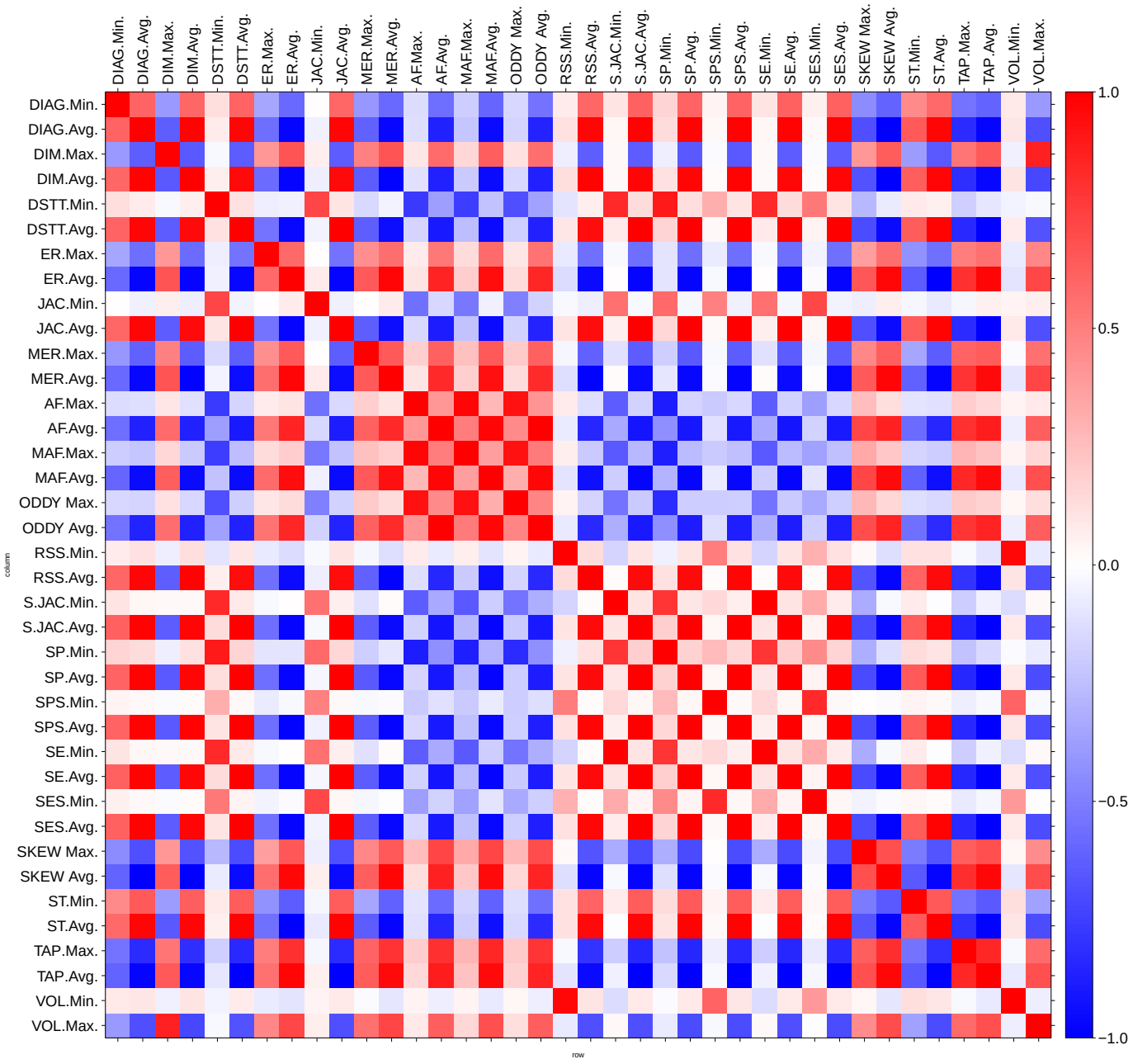

Fig. 18: The correlation matrix of the 38 metrics for the canew model.

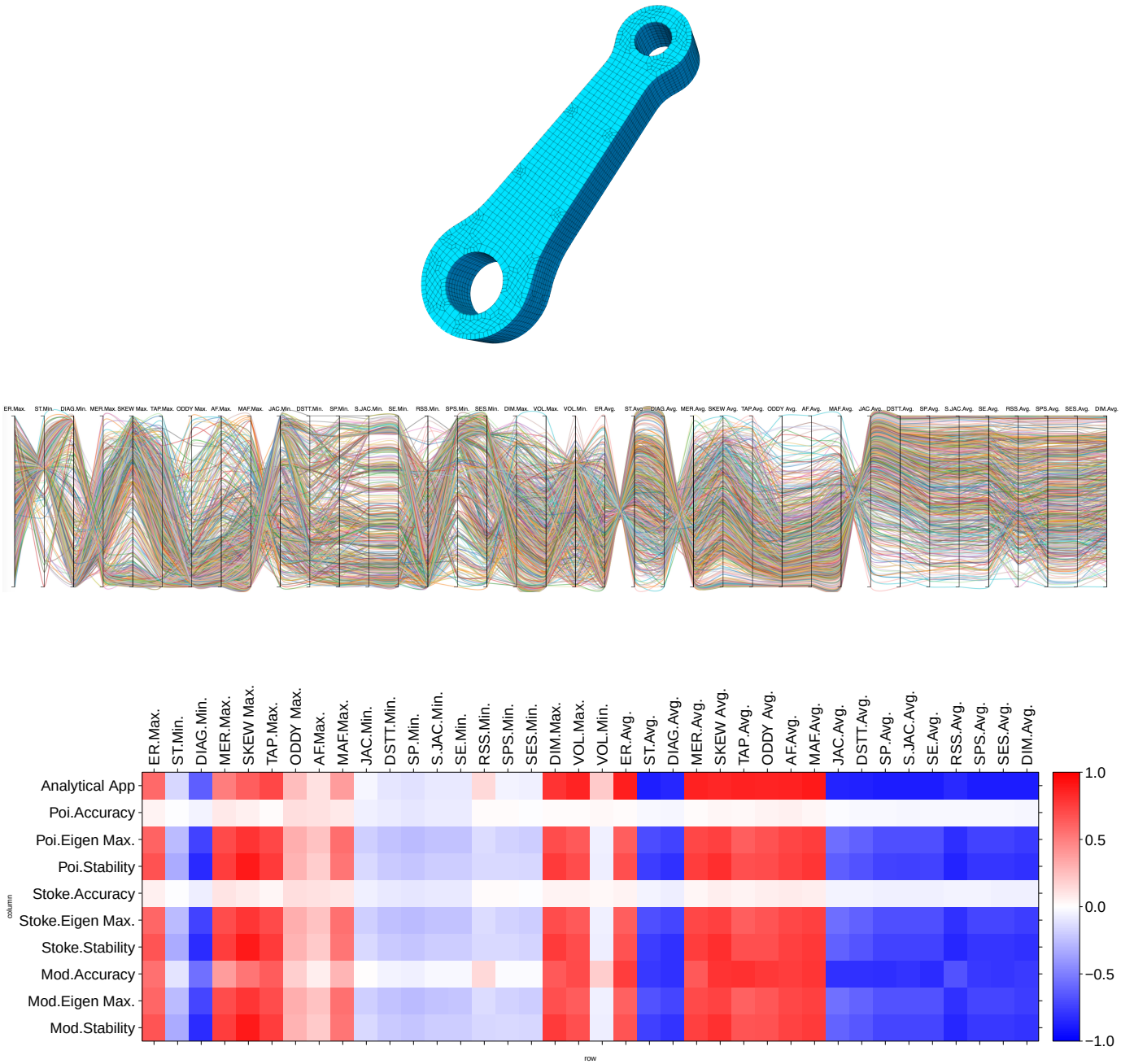

Fig. 19: The crank model (top), the parallel coordinate visualization of the sampled meshes (818 in total) in the metric space (middle), and the correlation matrix of the 38 metrics versus the Accuracy, Stability, and the difference of the solved maximal eigenvalue from the ground-truth (i.e., Max.Eigen) for the three simulations and the analytical application (bottom).

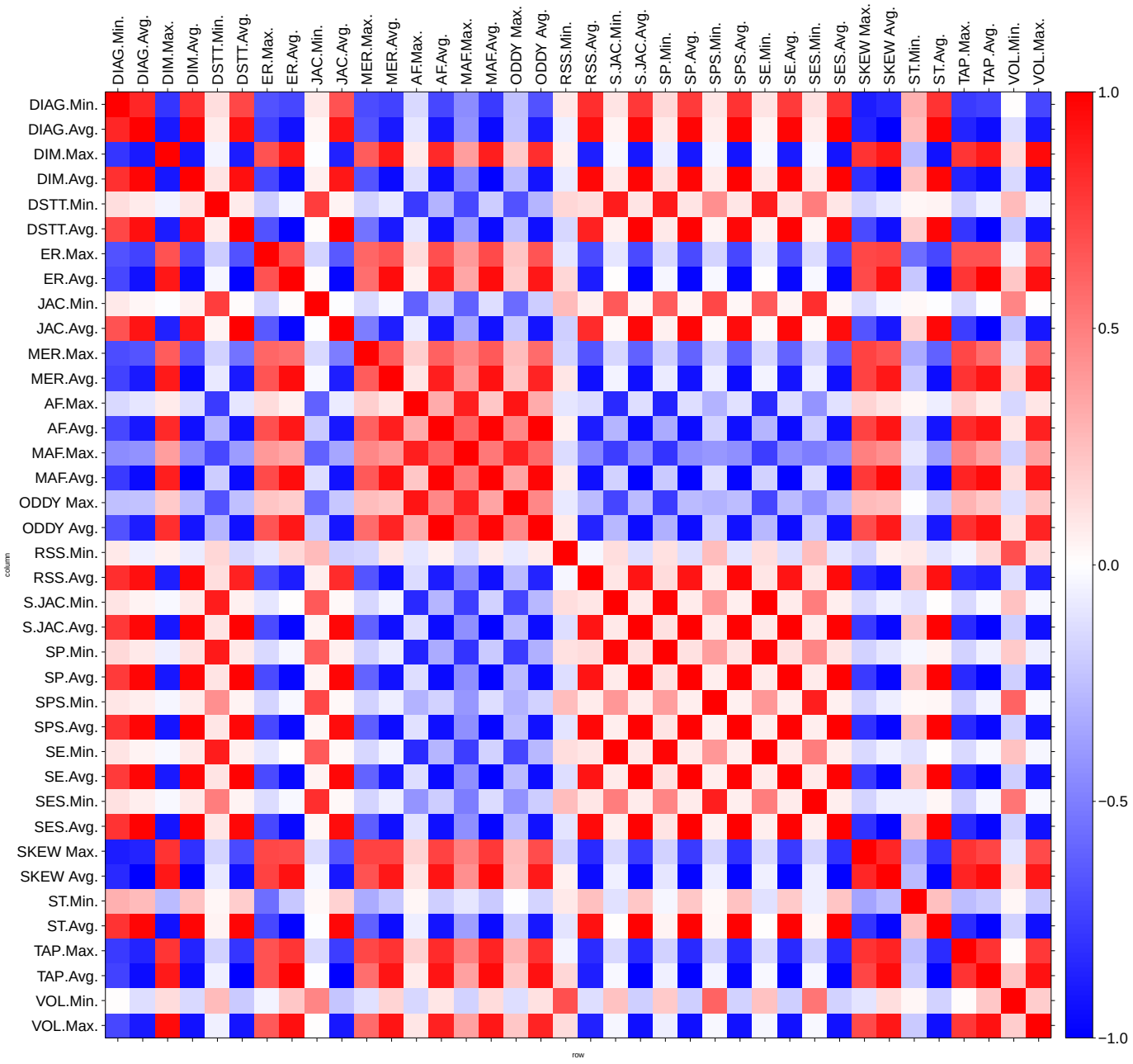

Fig. 20: The correlation matrix of the 38 metrics for the crank model.

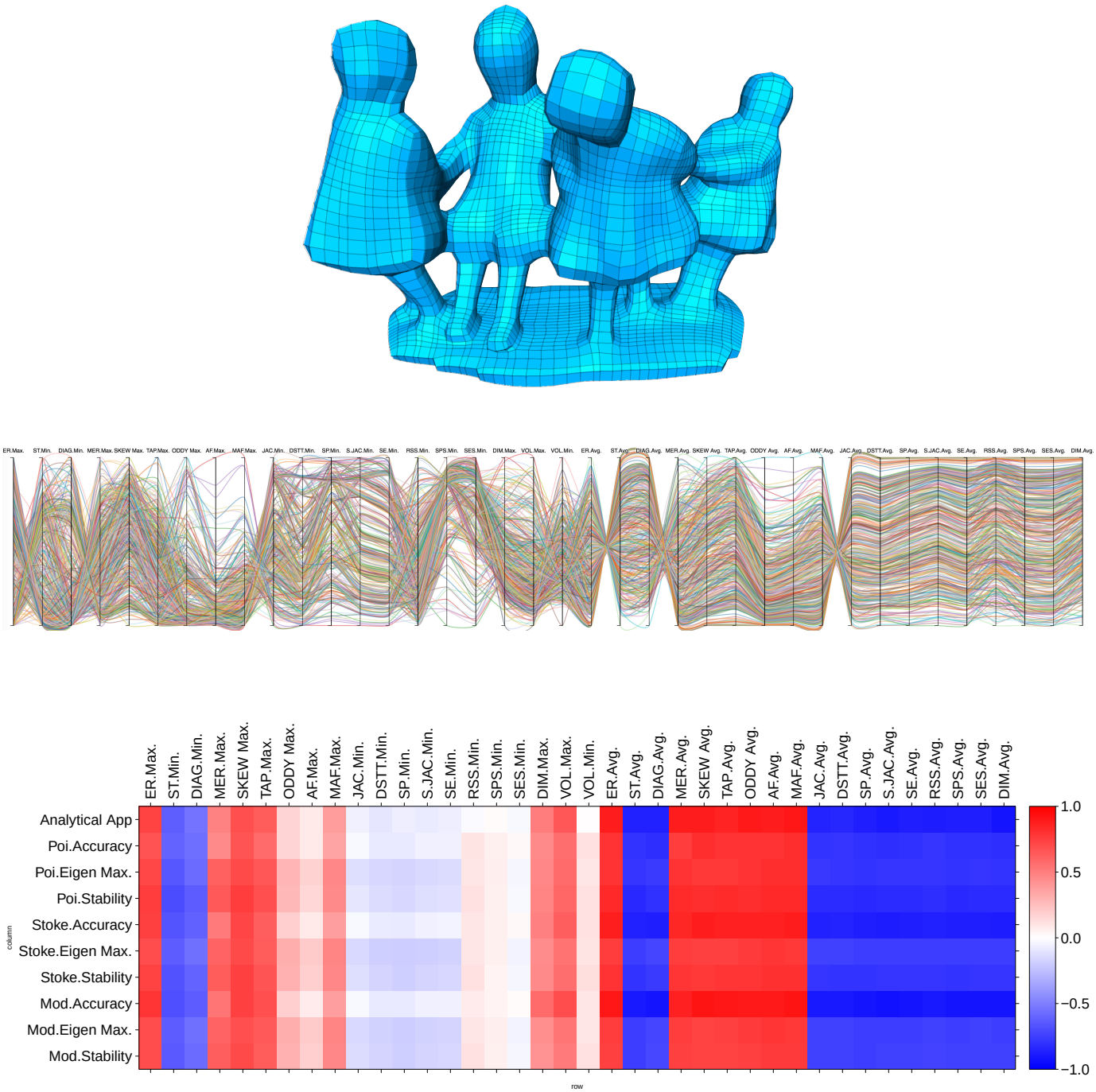

Fig. 21: The dancing children model (top), the parallel coordinate visualization of the sampled meshes (618 in total) in the metric space (middle), and the correlation matrix of the 38 metrics versus the Accuracy, Stability, and the difference of the solved maximal eigenvalue from the ground-truth (i.e., Max.Eigen) for the three simulations and the analytical application (bottom).

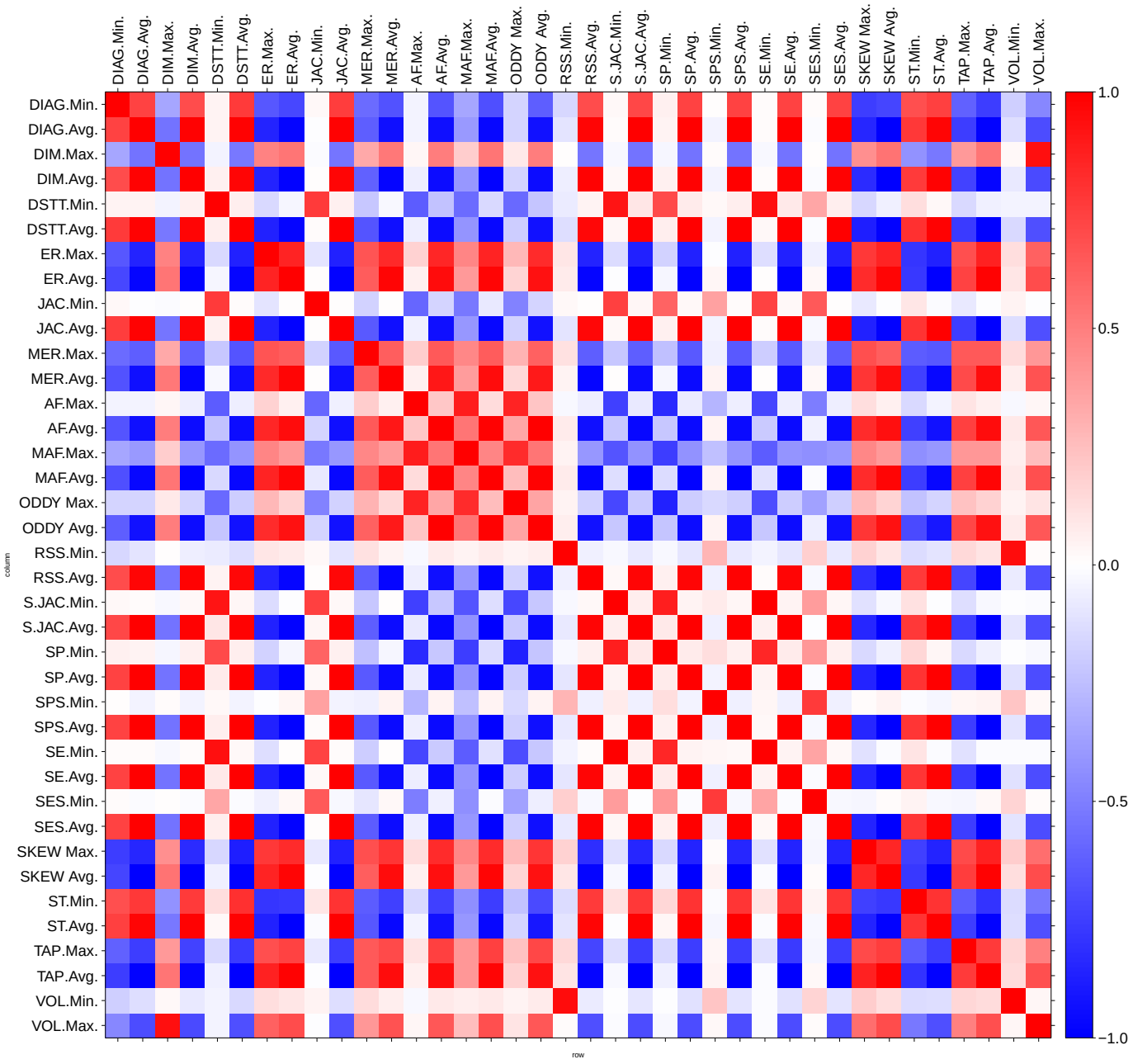

Fig. 22: The correlation matrix of the 38 metrics for the dancing children model.

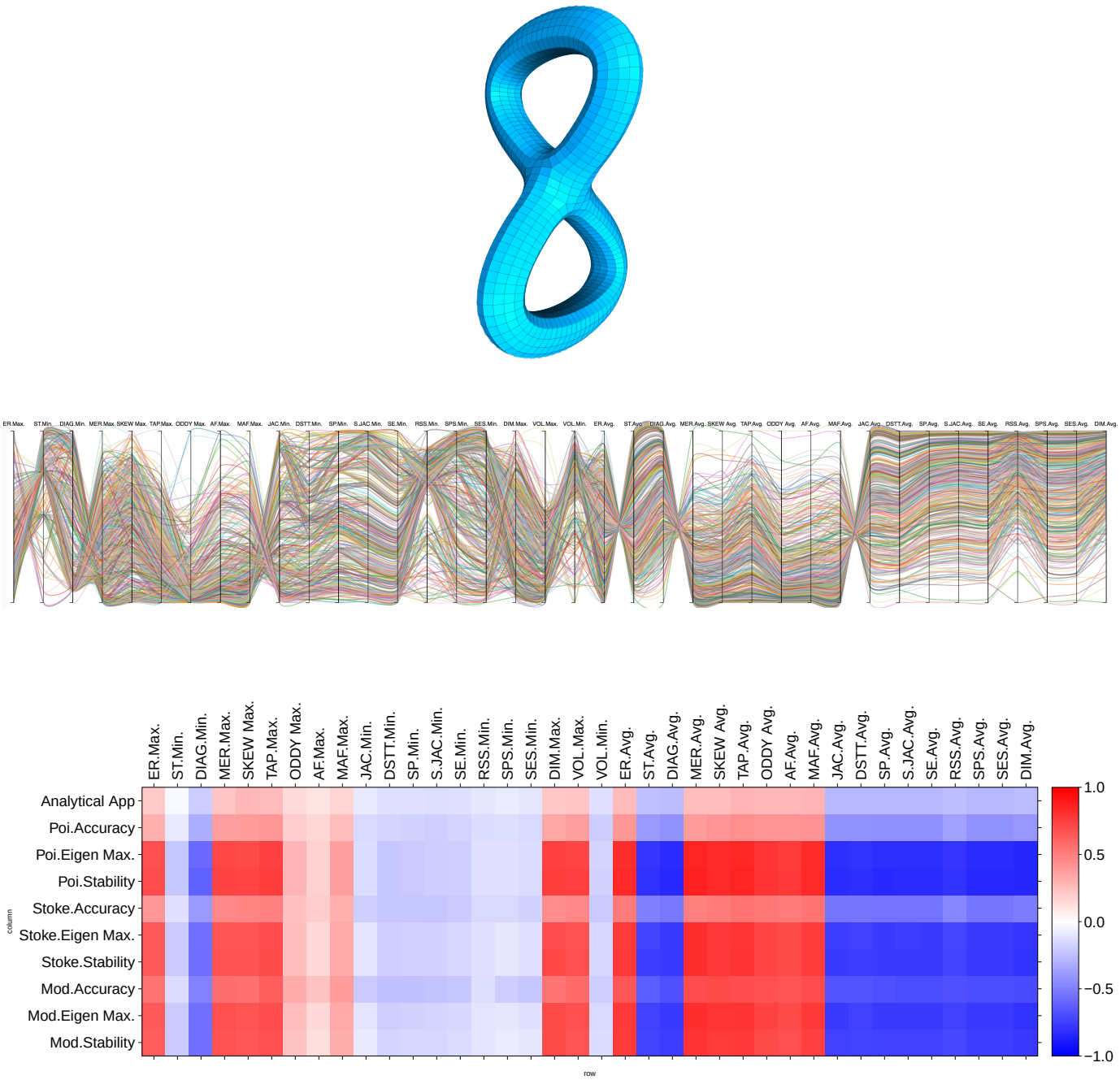

Fig. 23: Double torus (top), the parallel coordinate visualization of the sampled meshes (633 in total) in the metric space (middle), and the correlation matrix of the 38 metrics versus the Accuracy, Stability, and the difference of the solved maximal eigenvalue from the ground-truth (i.e., Max.Eigen) for the three simulations and the analytical application (bottom).

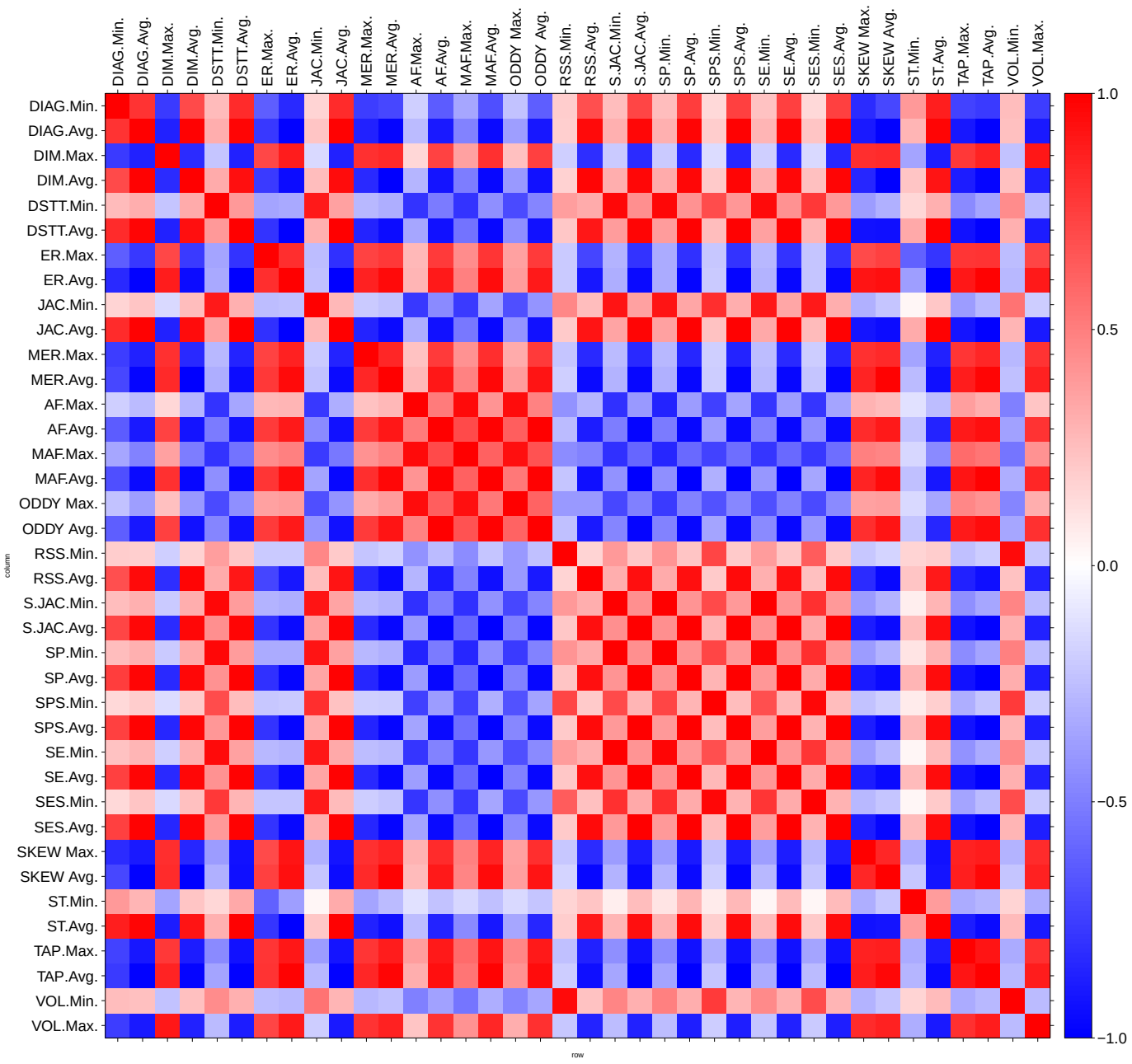

Fig. 24: The correlation matrix of the 38 metrics for the double torus.

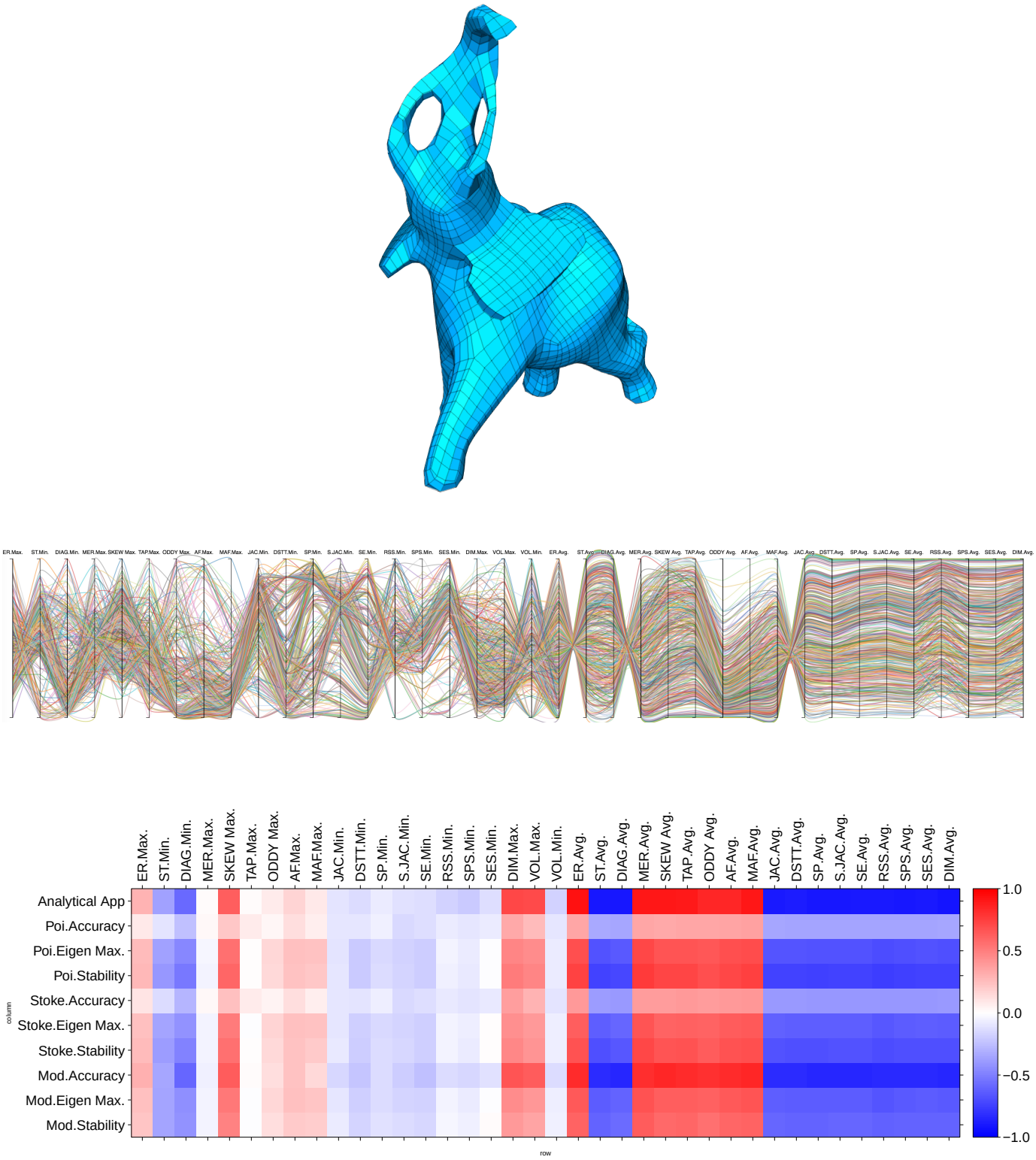

Fig. 25: The elephant model (top), the parallel coordinate visualization of the sampled meshes (643 in total) in the metric space (middle), and the correlation matrix of the 38 metrics versus the Accuracy, Stability, and the difference of the solved maximal eigenvalue from the ground-truth (i.e., Max.Eigen) for the three simulations and the analytical application (bottom).

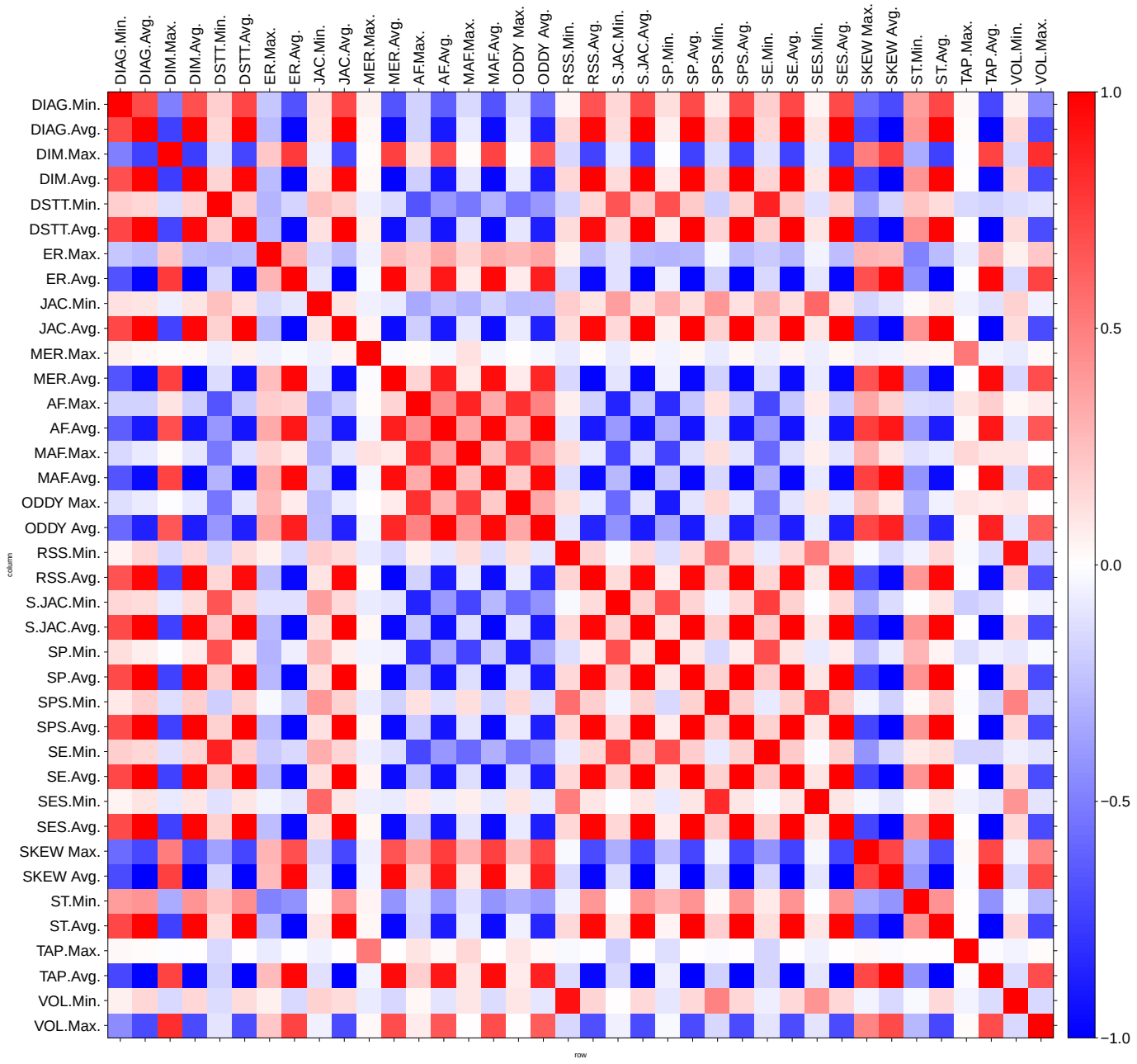

Fig. 26: The correlation matrix of the 38 metrics for the elephant model.

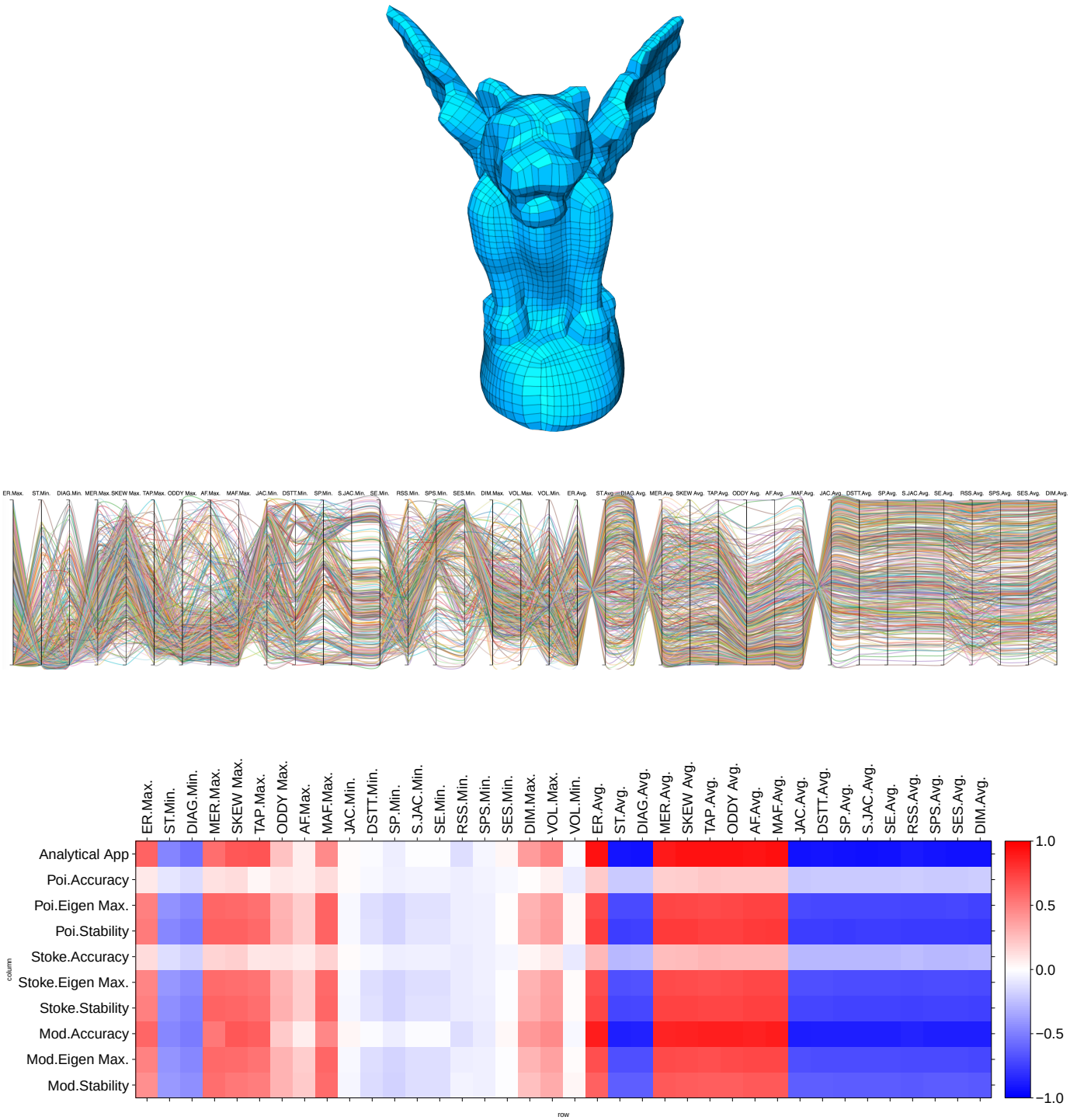

Fig. 27: The gargoyle model (top), the parallel coordinate visualization of the sampled meshes (616 in total) in the metric space (middle), and the correlation matrix of the 38 metrics versus the Accuracy, Stability, and the difference of the solved maximal eigenvalue from the ground-truth (i.e., Max.Eigen) for the three simulations and the analytical application (bottom).

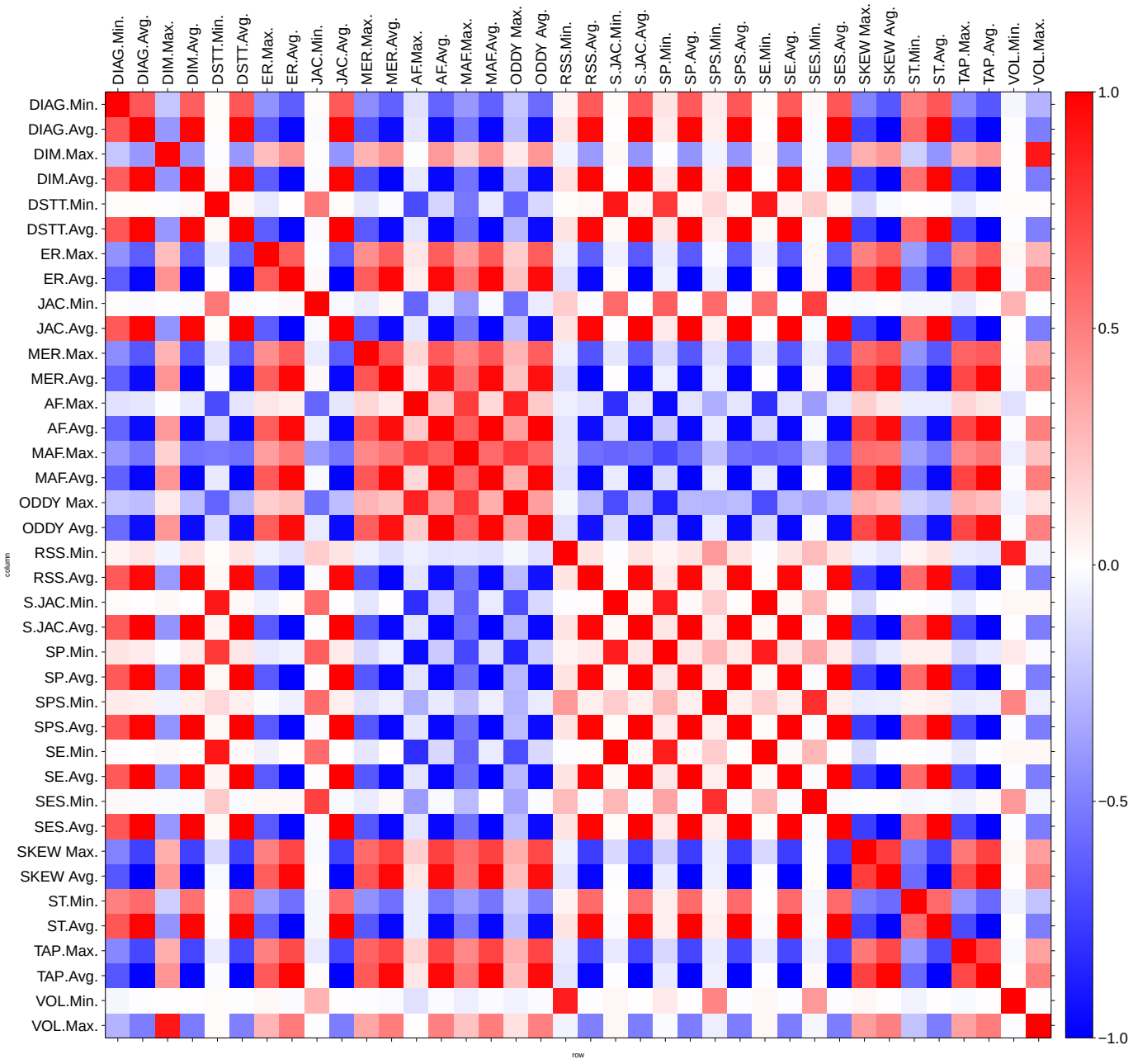

Fig. 28: The correlation matrix of the 38 metrics for the gargoyle model.

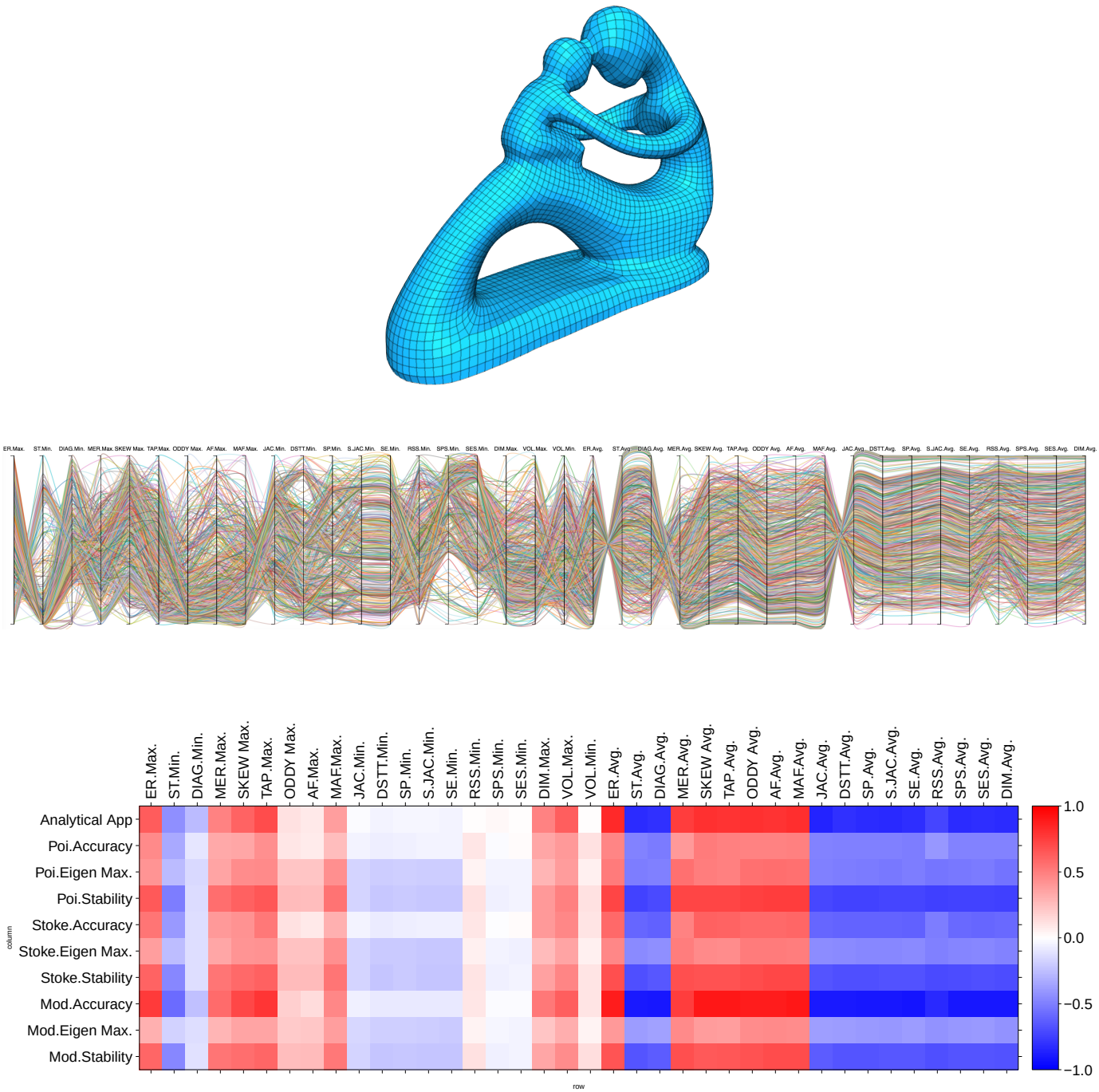

Fig. 29: The fertility model (top), the parallel coordinate visualization of the sampled meshes (817 in total) in the metric space (middle), and the correlation matrix of the 38 metrics versus the Accuracy, Stability, and the difference of the solved maximal eigenvalue from the ground-truth (i.e., Max.Eigen) for the three simulations and the analytical application (bottom).

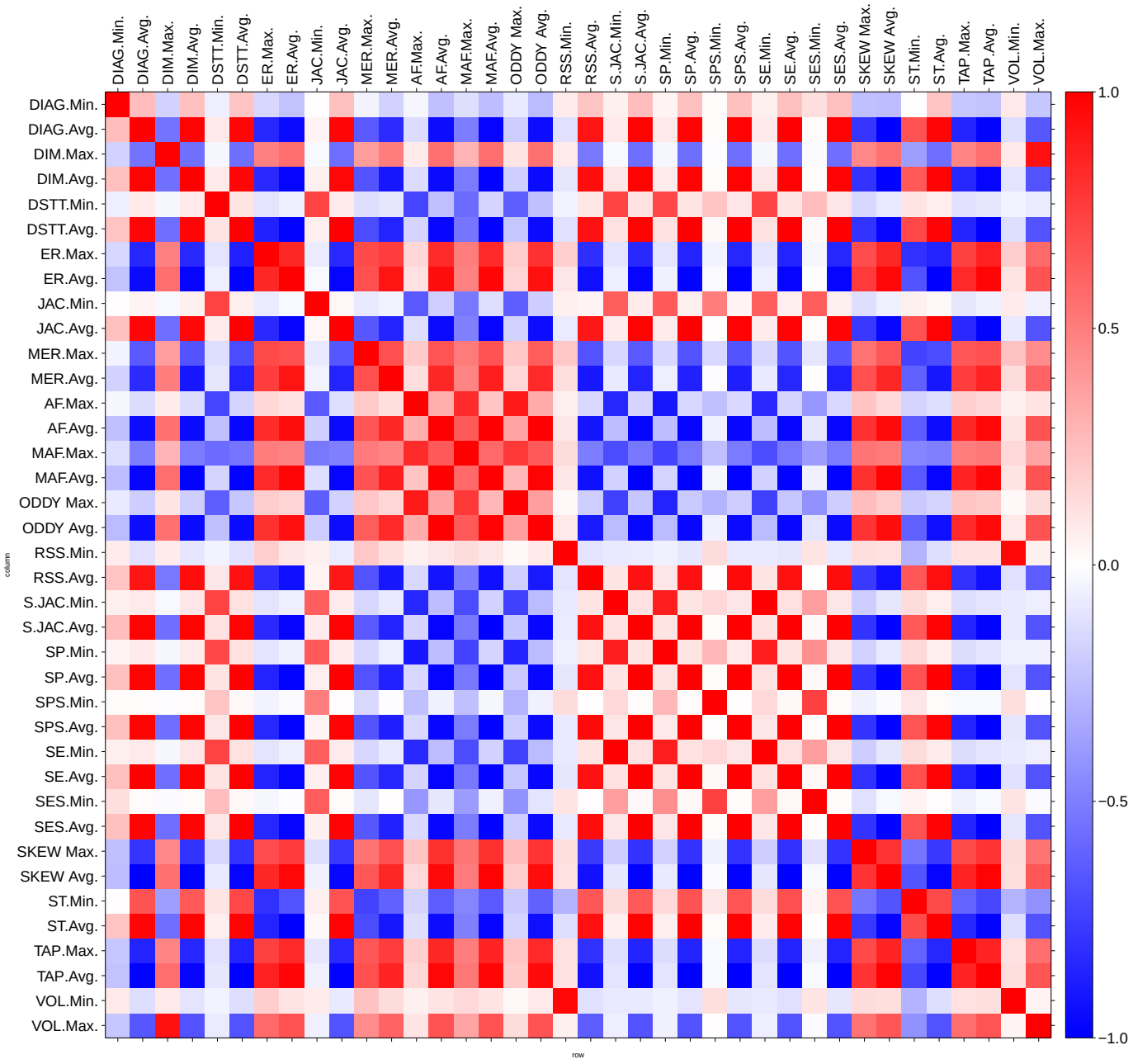

Fig. 30: The correlation matrix of the 38 metrics for the fertility model.

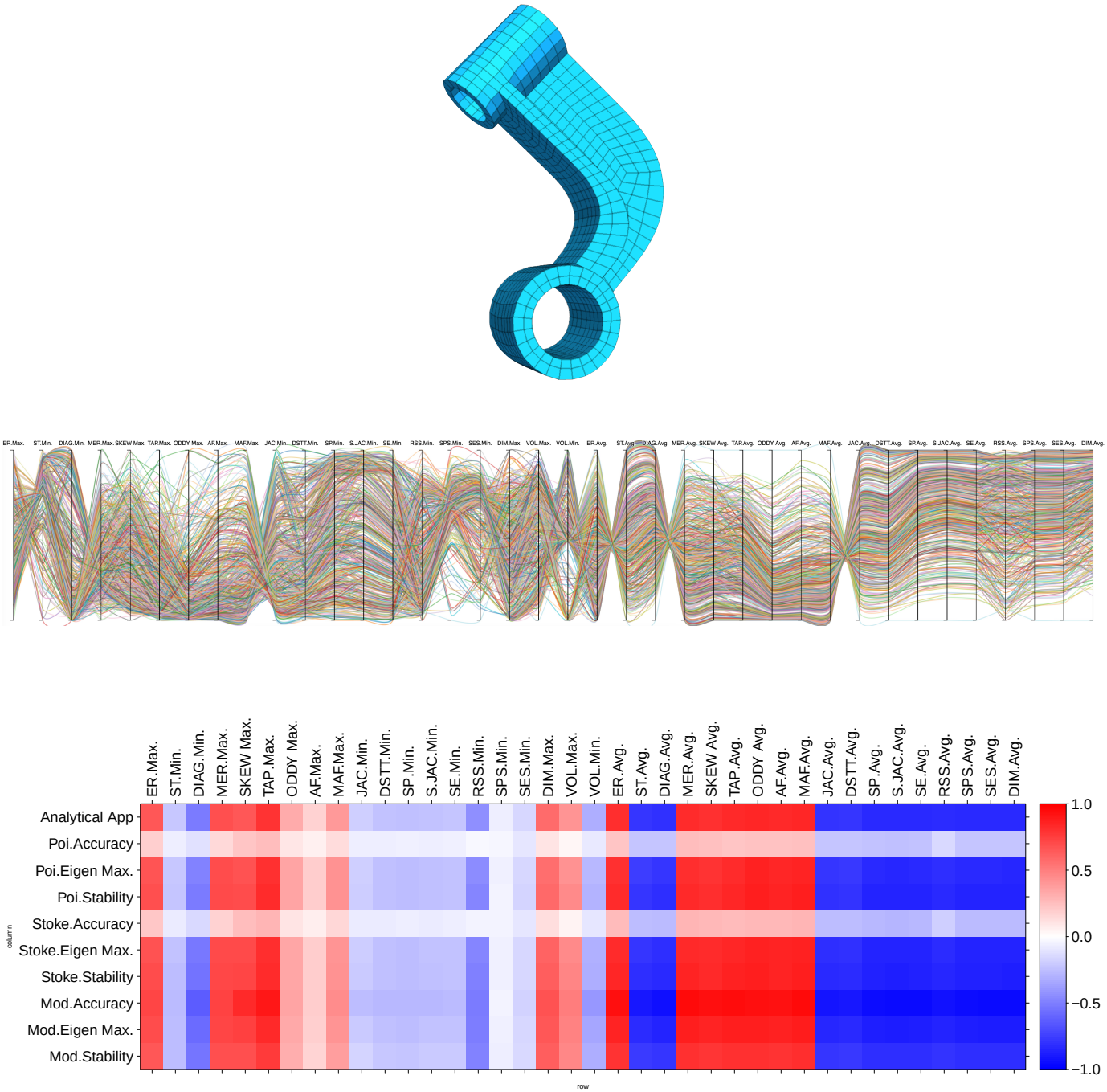

Fig. 31: The hanger model (top), the parallel coordinate visualization of the sampled meshes (719 in total) in the metric space (middle), and the correlation matrix of the 38 metrics versus the Accuracy, Stability, and the difference of the solved maximal eigenvalue from the ground-truth (i.e., Max.Eigen) for the three simulations and the analytical application (bottom).

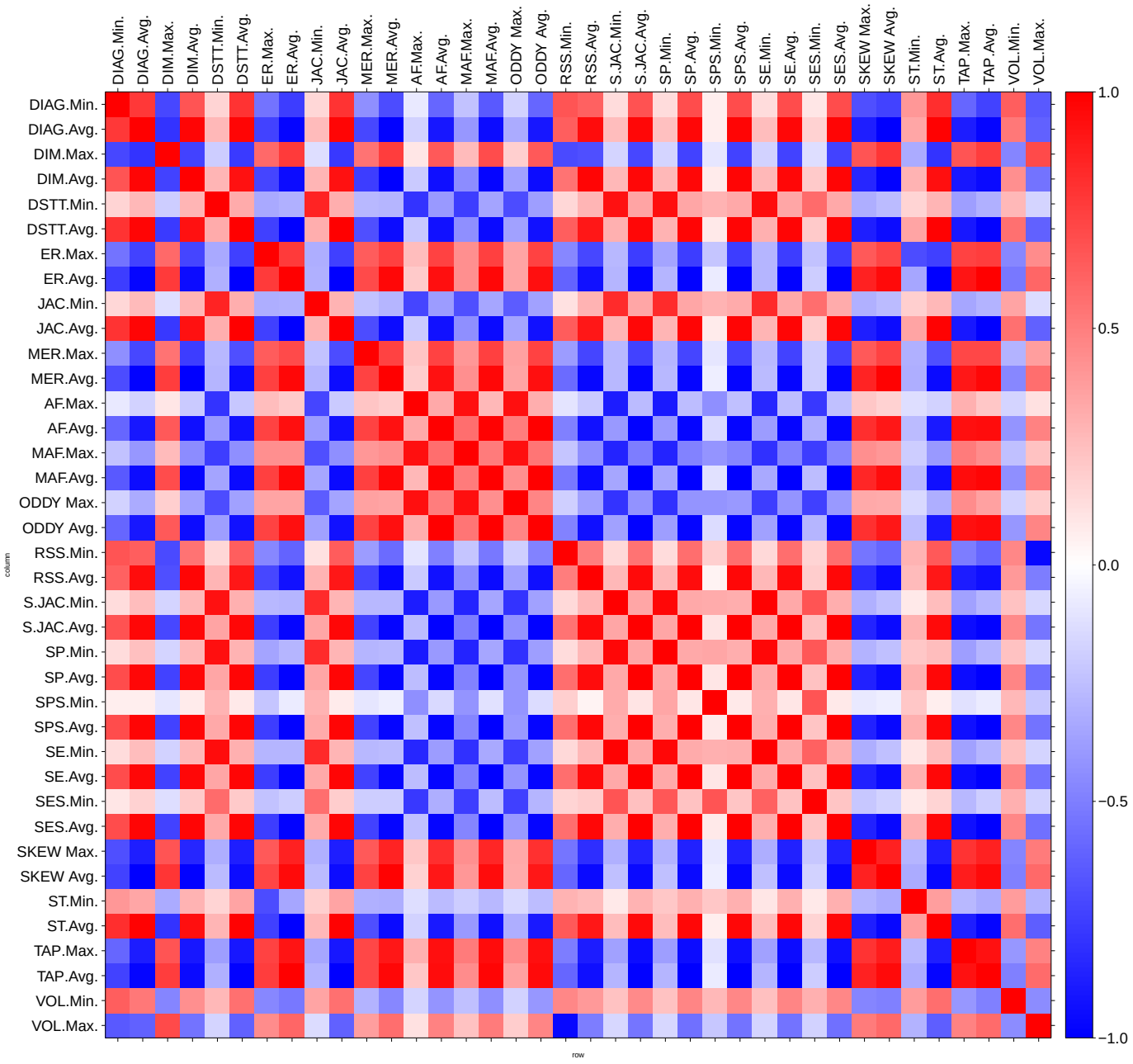

Fig. 32: The correlation matrix of the 38 metrics for the hanger model.

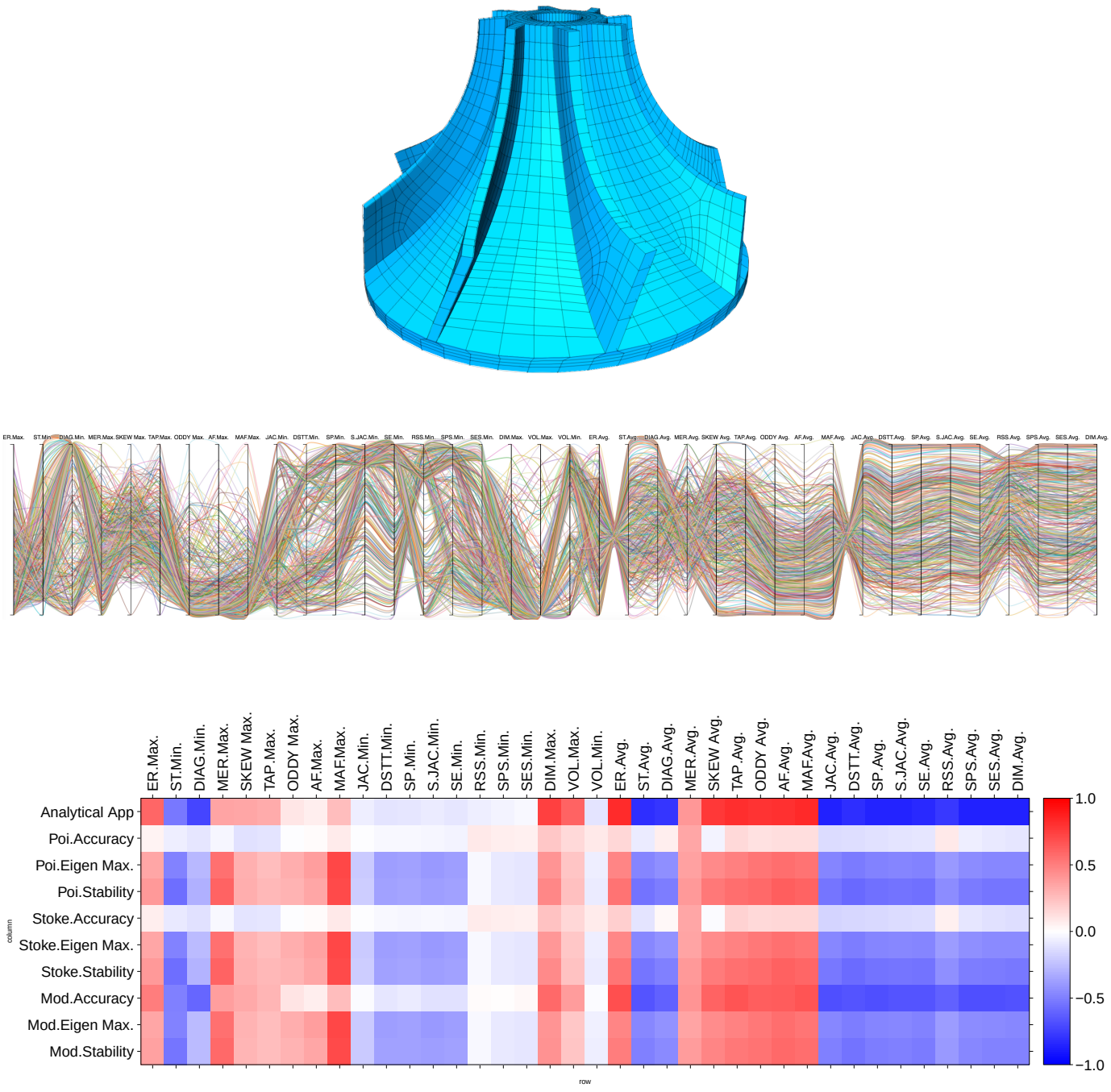

Fig. 33: The impeller model (top), the parallel coordinate visualization of the sampled meshes (619 in total) in the metric space (middle), and the correlation matrix of the 38 metrics versus the Accuracy, Stability, and the difference of the solved maximal eigenvalue from the ground-truth (i.e., Max.Eigen) for the three simulations and the analytical application (bottom).

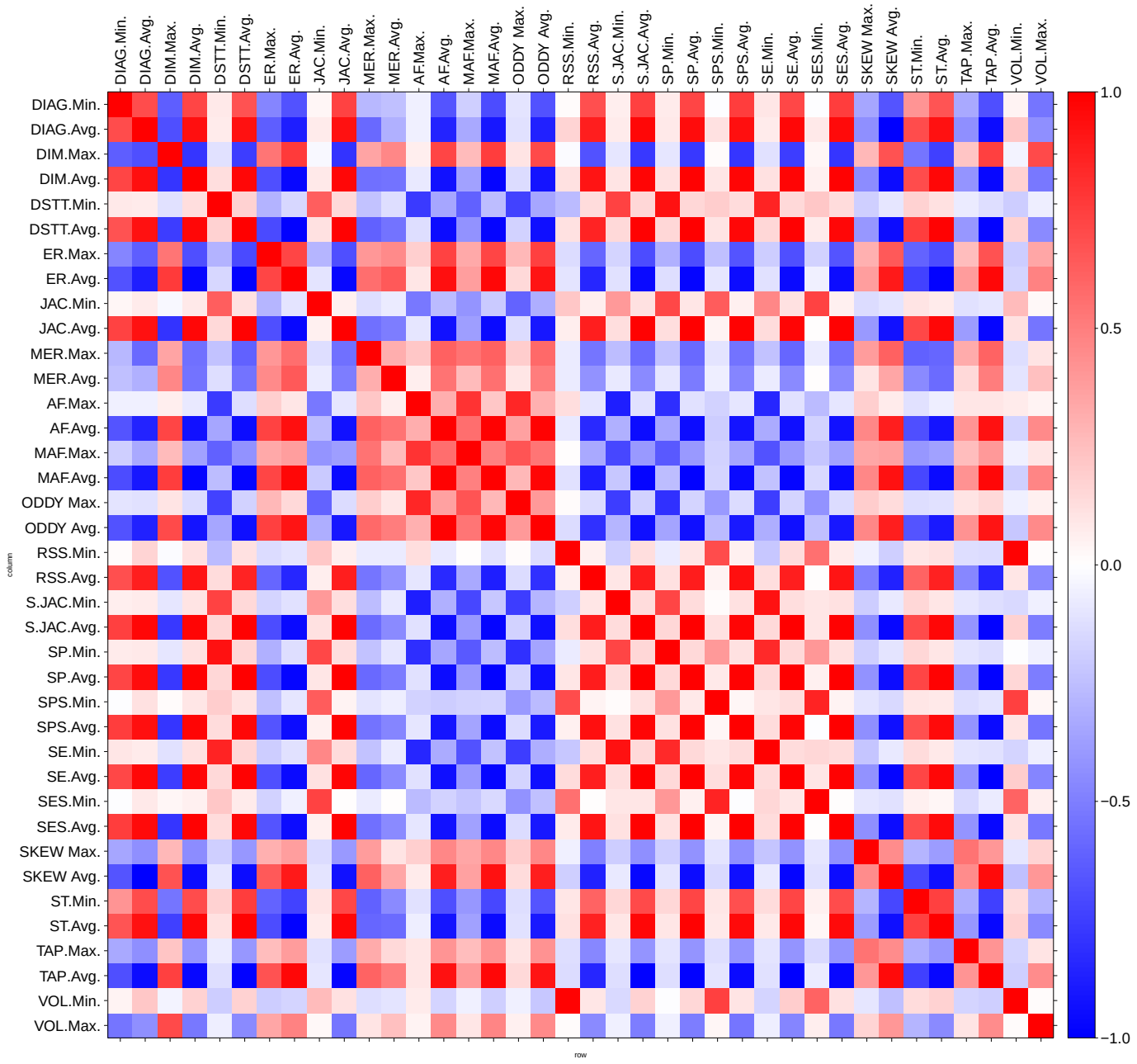

Fig. 34: The correlation matrix of the 38 metrics for the impeller model.

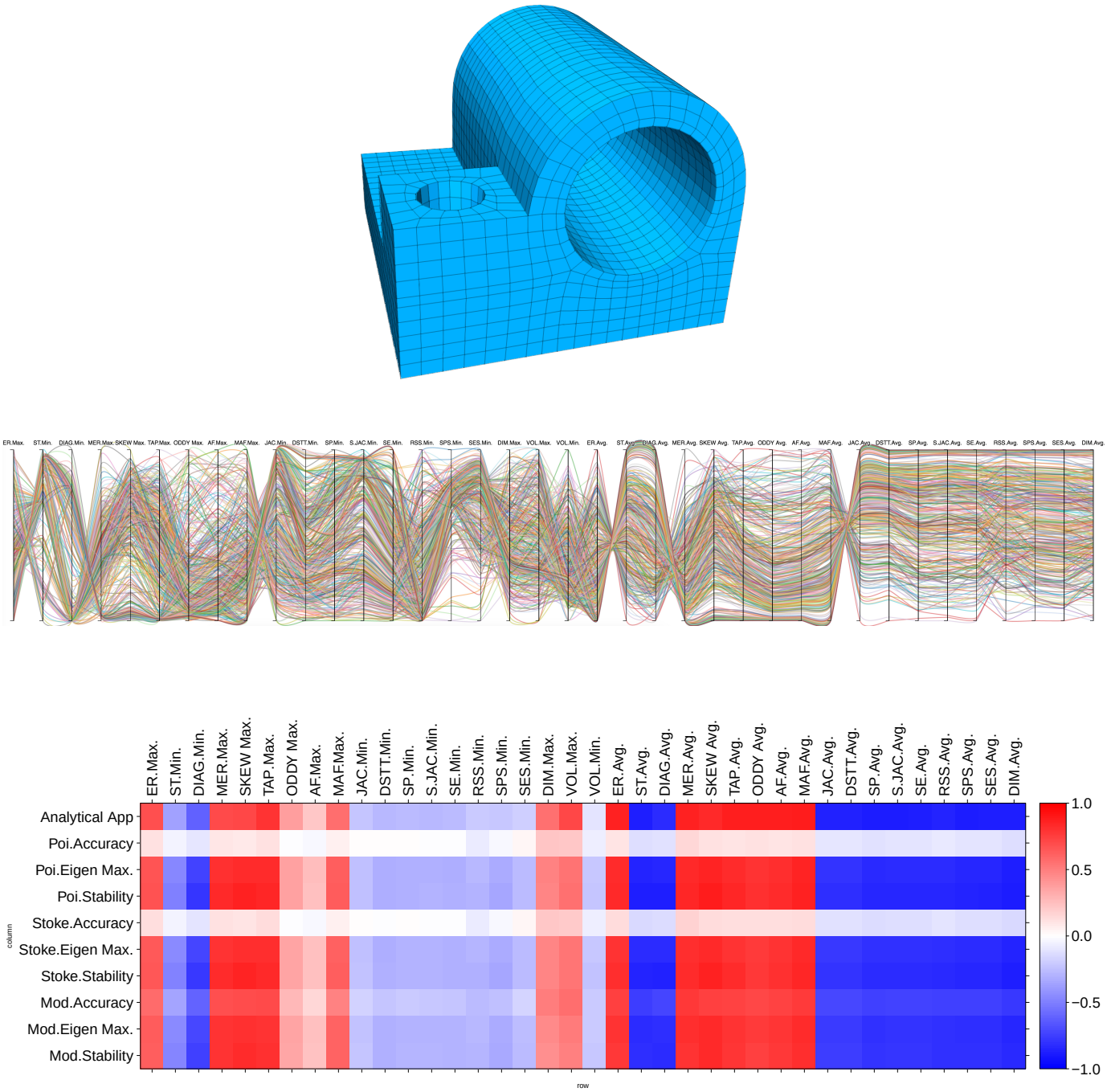

Fig. 35: The joint model (top), the parallel coordinate visualization of the sampled meshes (586 in total) in the metric space (middle), and the correlation matrix of the 38 metrics versus the Accuracy, Stability, and the difference of the solved maximal eigenvalue from the ground-truth (i.e., Max.Eigen) for the three simulations and the analytical application (bottom).

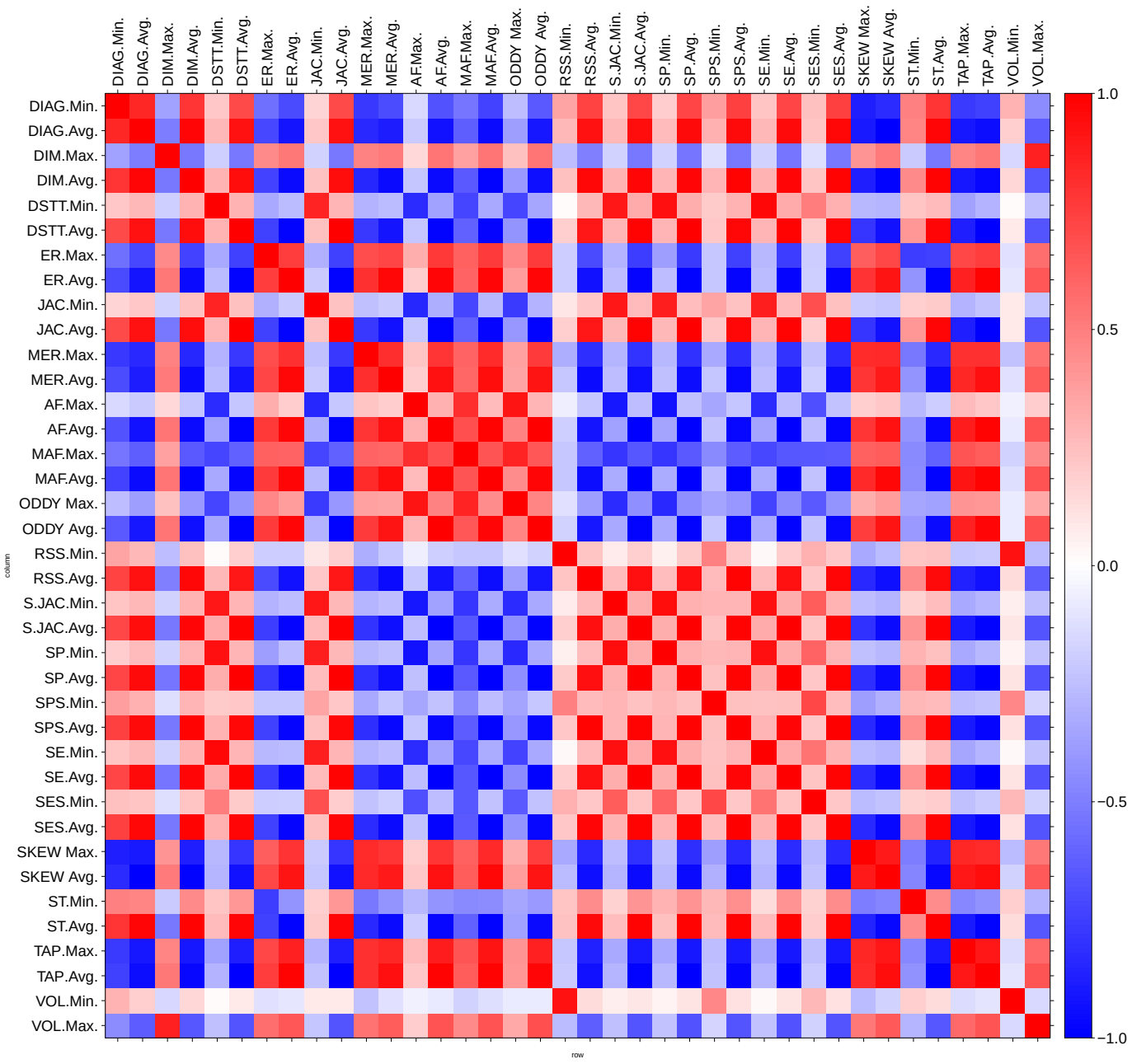

Fig. 36: The correlation matrix of the 38 metrics for the joint model.

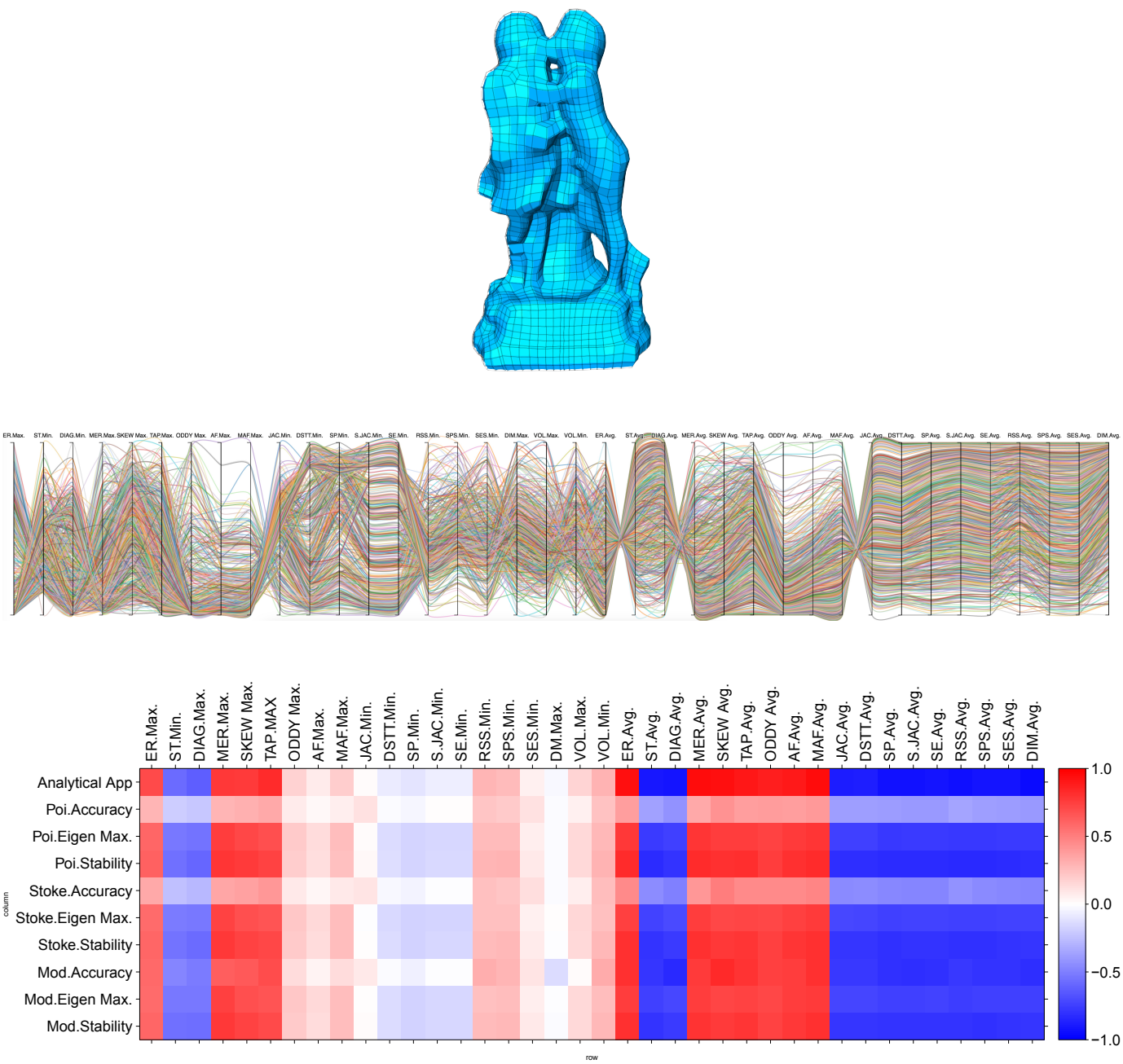

Fig. 37: The kiss model (top), the parallel coordinate visualization of the sampled meshes (828 in total) in the metric space (middle), and the correlation matrix of the 38 metrics versus the Accuracy, Stability, and the difference of the solved maximal eigenvalue from the ground-truth (i.e., Max.Eigen) for the three simulations and the analytical application (bottom).

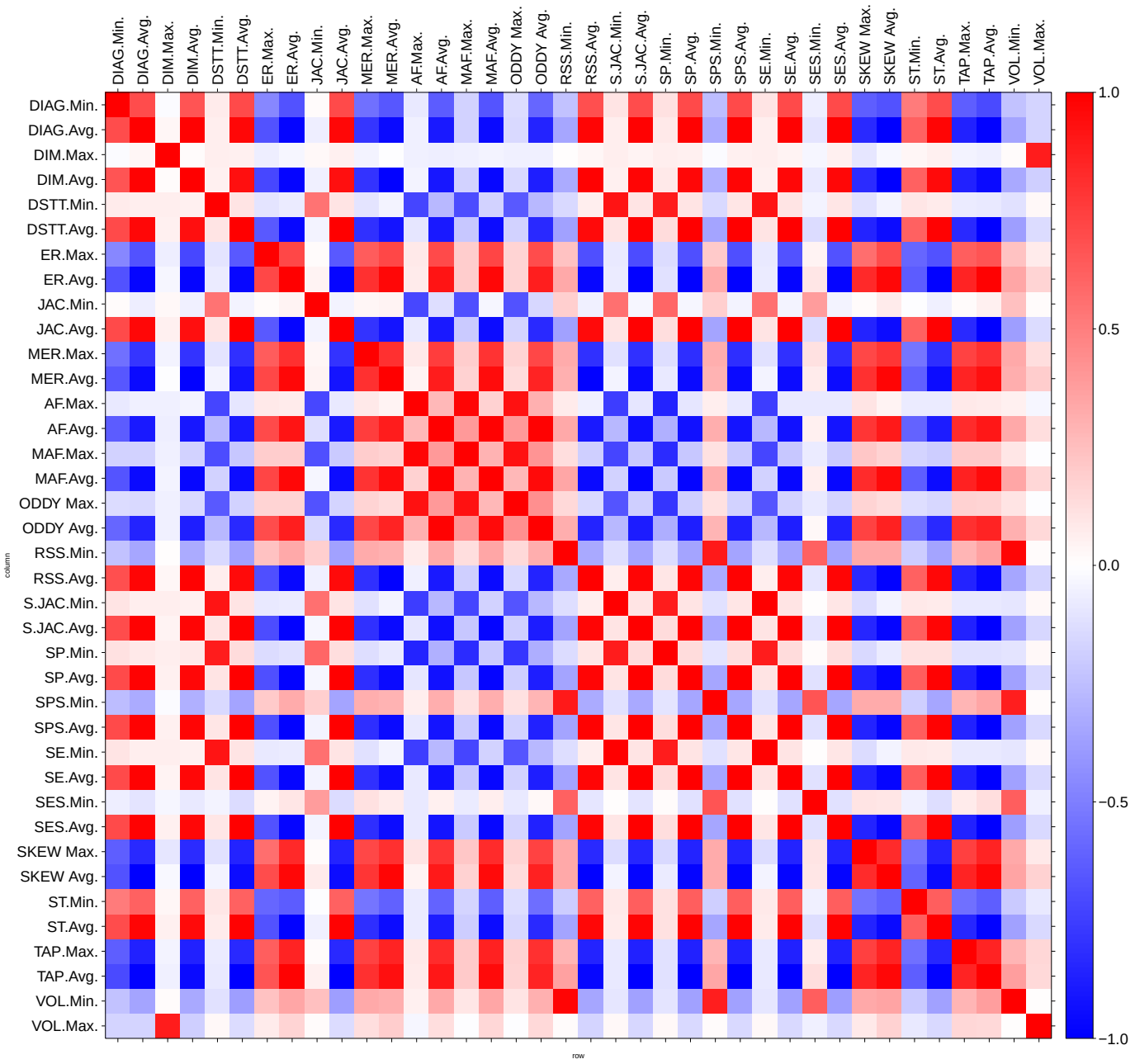

Fig. 38: The correlation matrix of the 38 metrics for the kiss model.

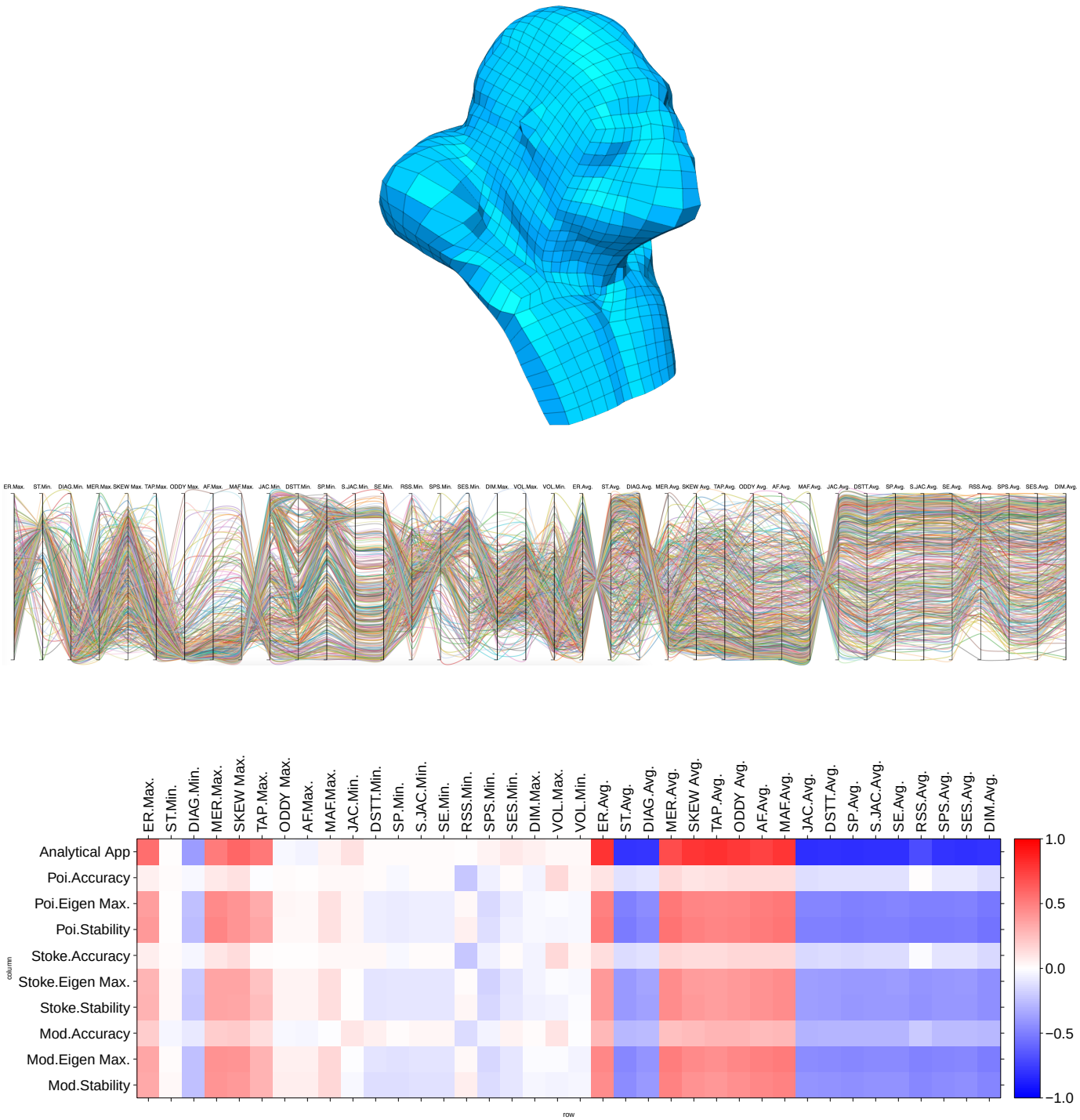

Fig. 39: The King Kong model (top), the parallel coordinate visualization of the sampled meshes (548 in total) in the metric space (middle), and the correlation matrix of the 38 metrics versus the Accuracy, Stability, and the difference of the solved maximal eigenvalue from the ground-truth (i.e., Max.Eigen) for the three simulations and the analytical application (bottom).

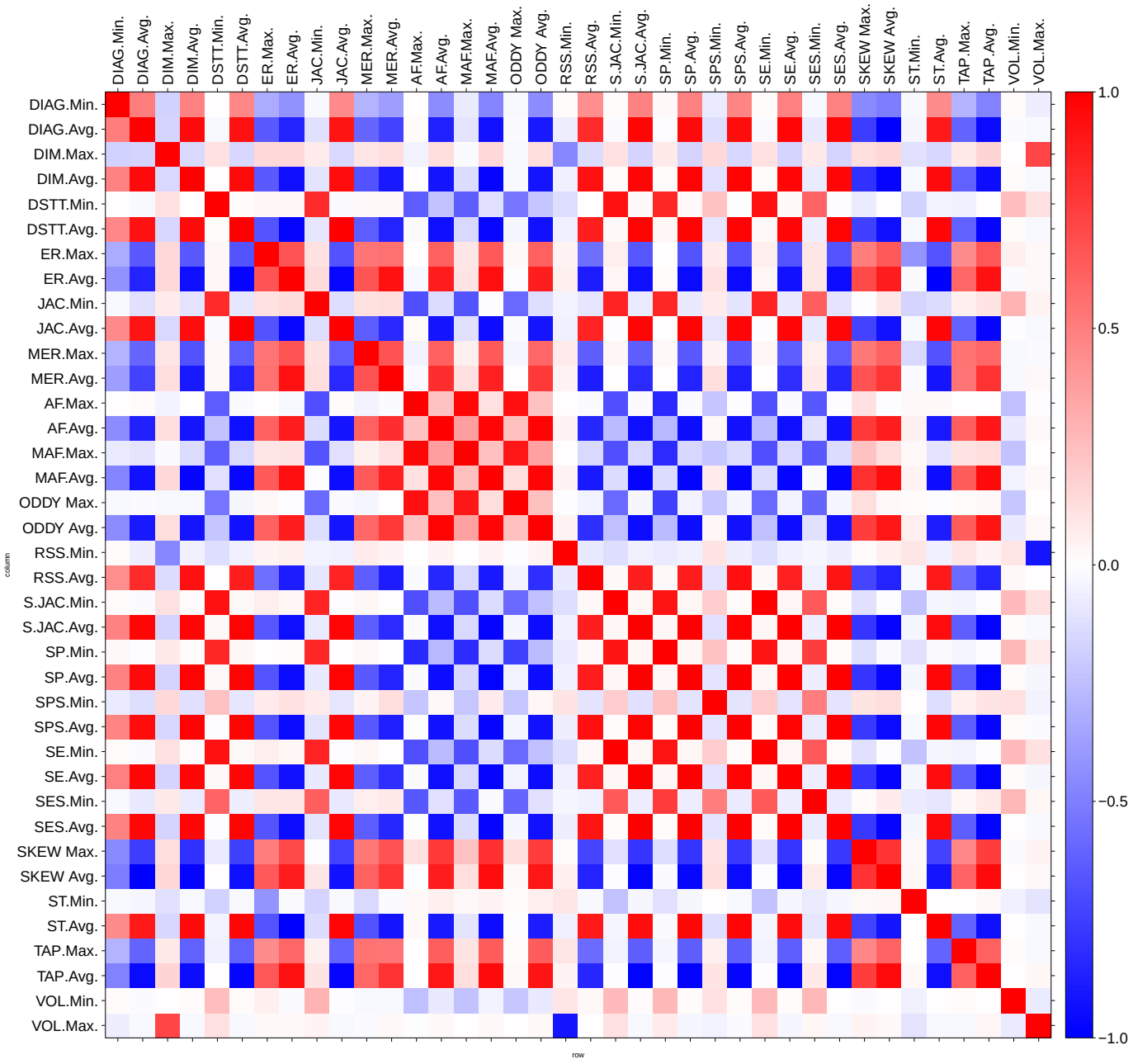

Fig. 40: The correlation matrix of the 38 metrics for the King Kong model.

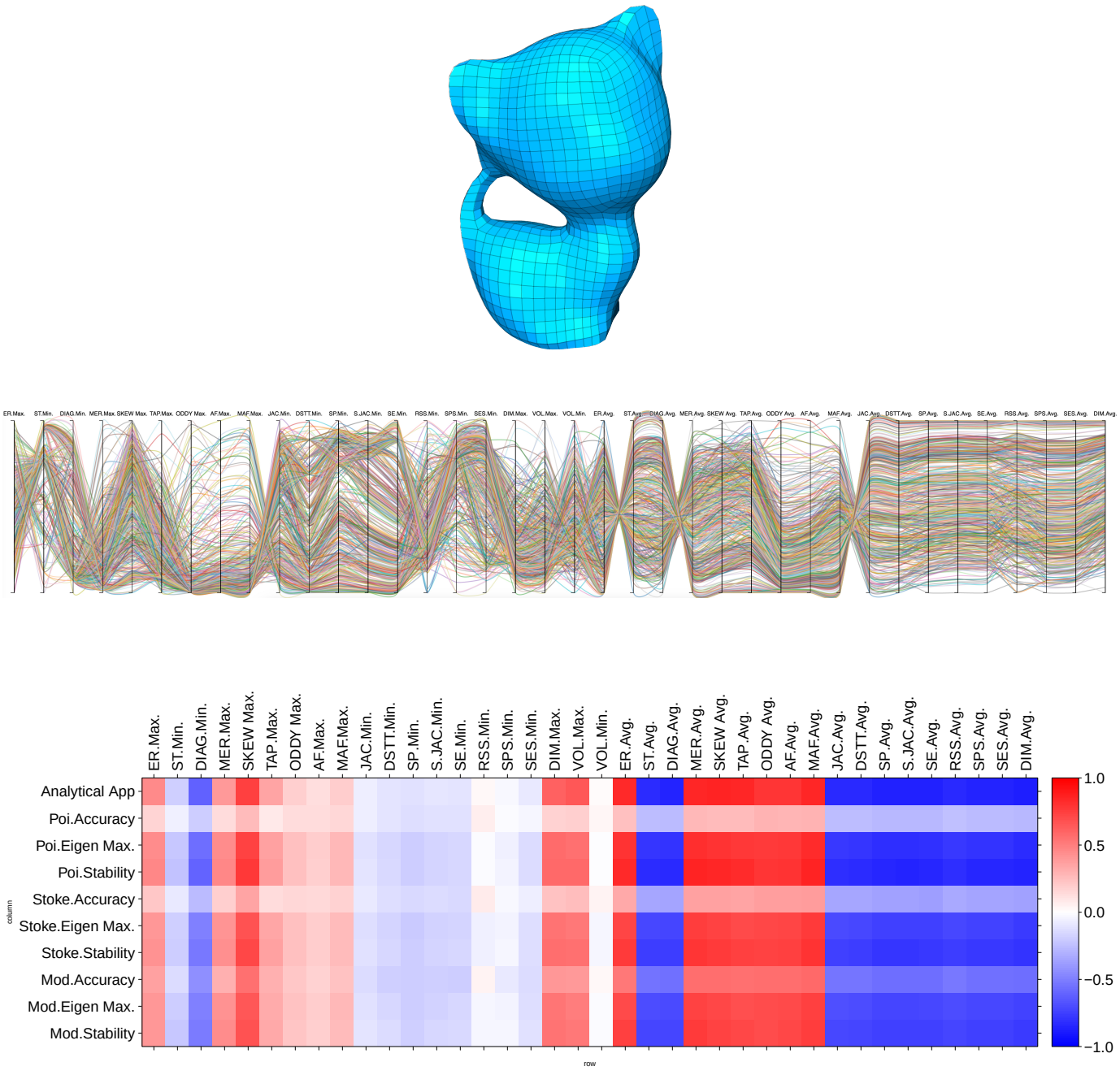

Fig. 41: The kitty model (top), the parallel coordinate visualization of the sampled meshes (692 in total) in the metric space (middle), and the correlation matrix of the 38 metrics versus the Accuracy, Stability, and the difference of the solved maximal eigenvalue from the ground-truth (i.e., Max.Eigen) for the three simulations and the analytical application (bottom).

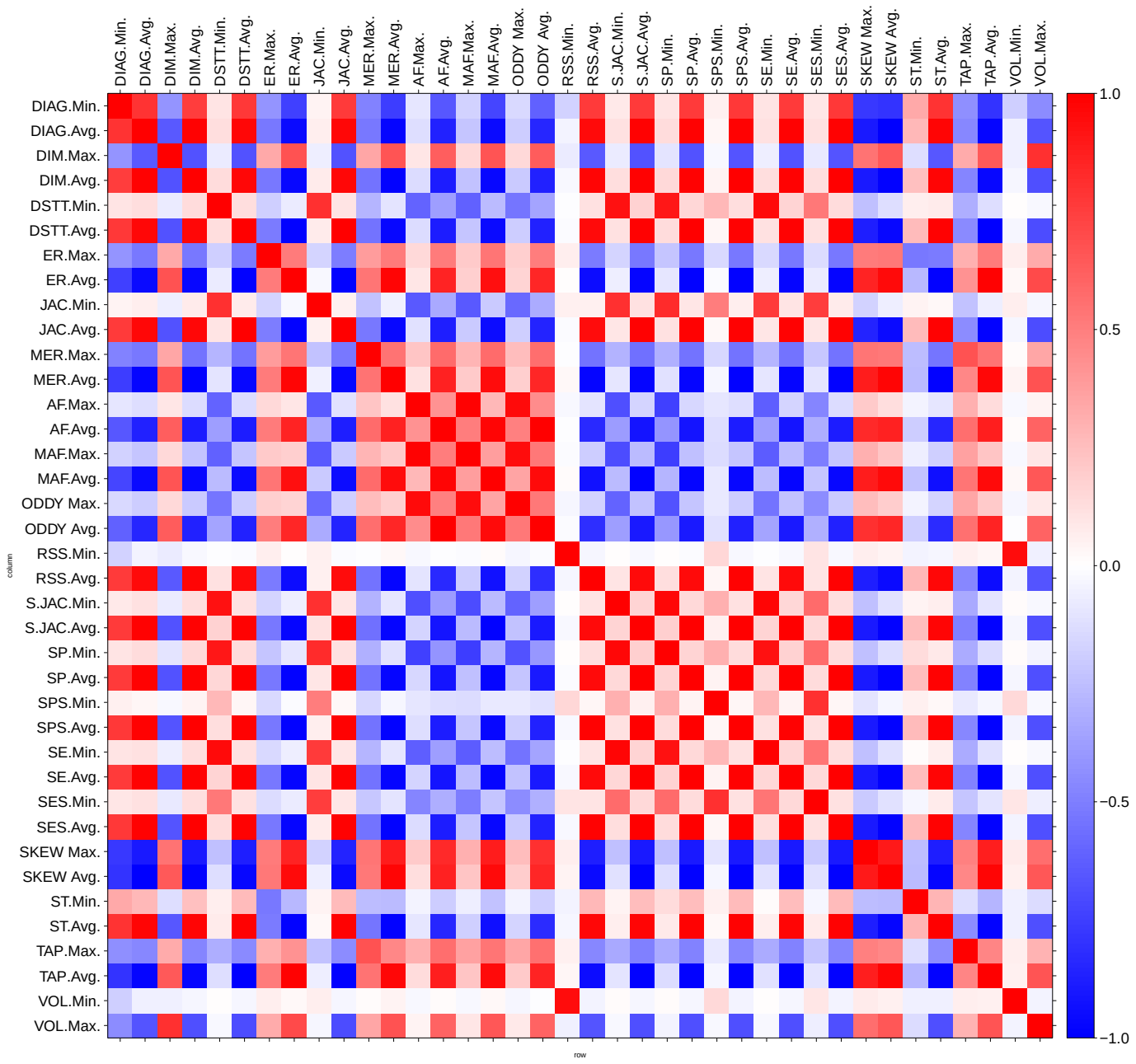

Fig. 42: The correlation matrix of the 38 metrics for the kitty model.

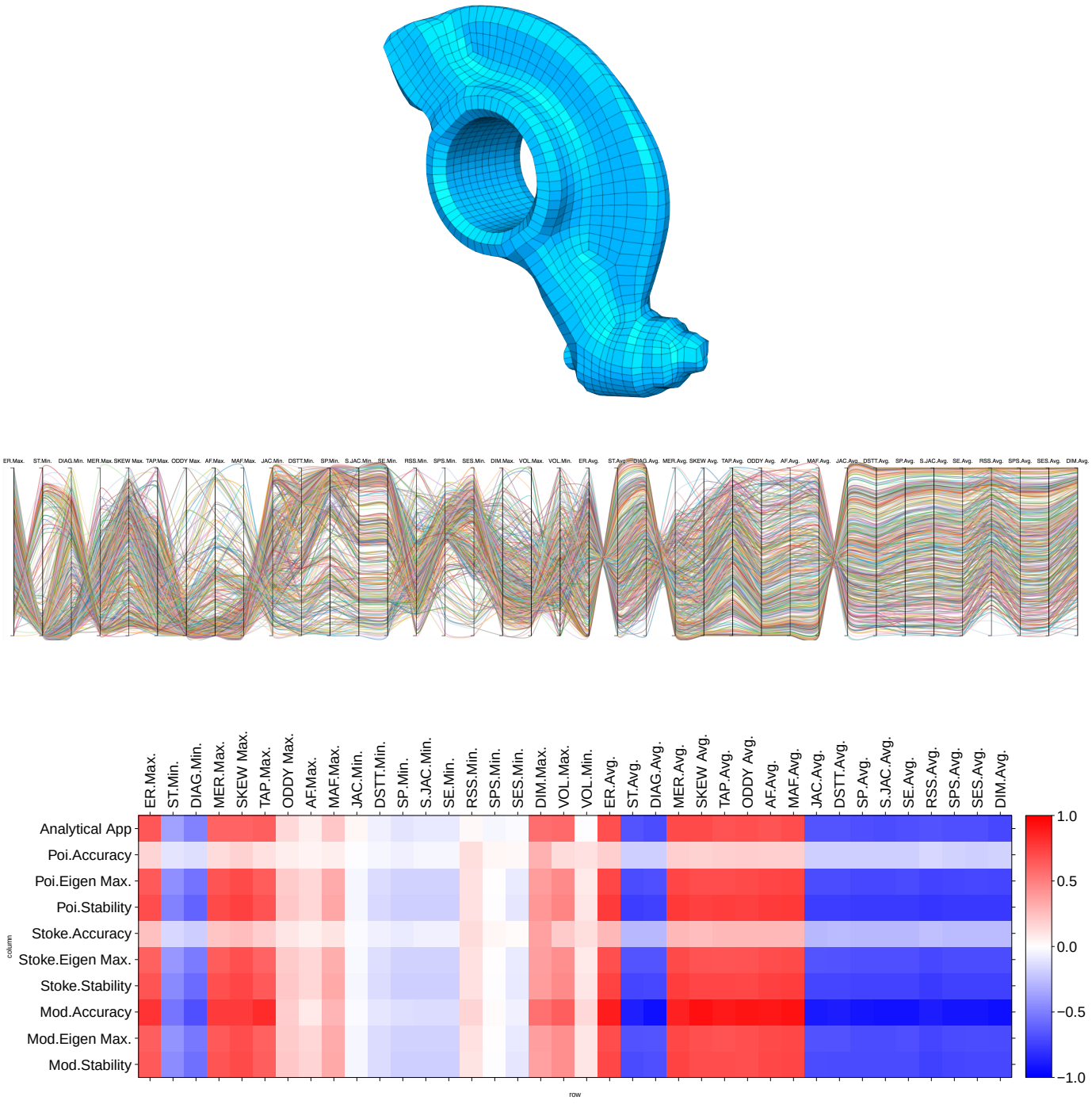

Fig. 43: The rockerarm model (top), the parallel coordinate visualization of the sampled meshes (565 in total) in the metric space (middle), and the correlation matrix of the 38 metrics versus the Accuracy, Stability, and the difference of the solved maximal eigenvalue from the ground-truth (i.e., Max.Eigen) for the three simulations and the analytical application (bottom).

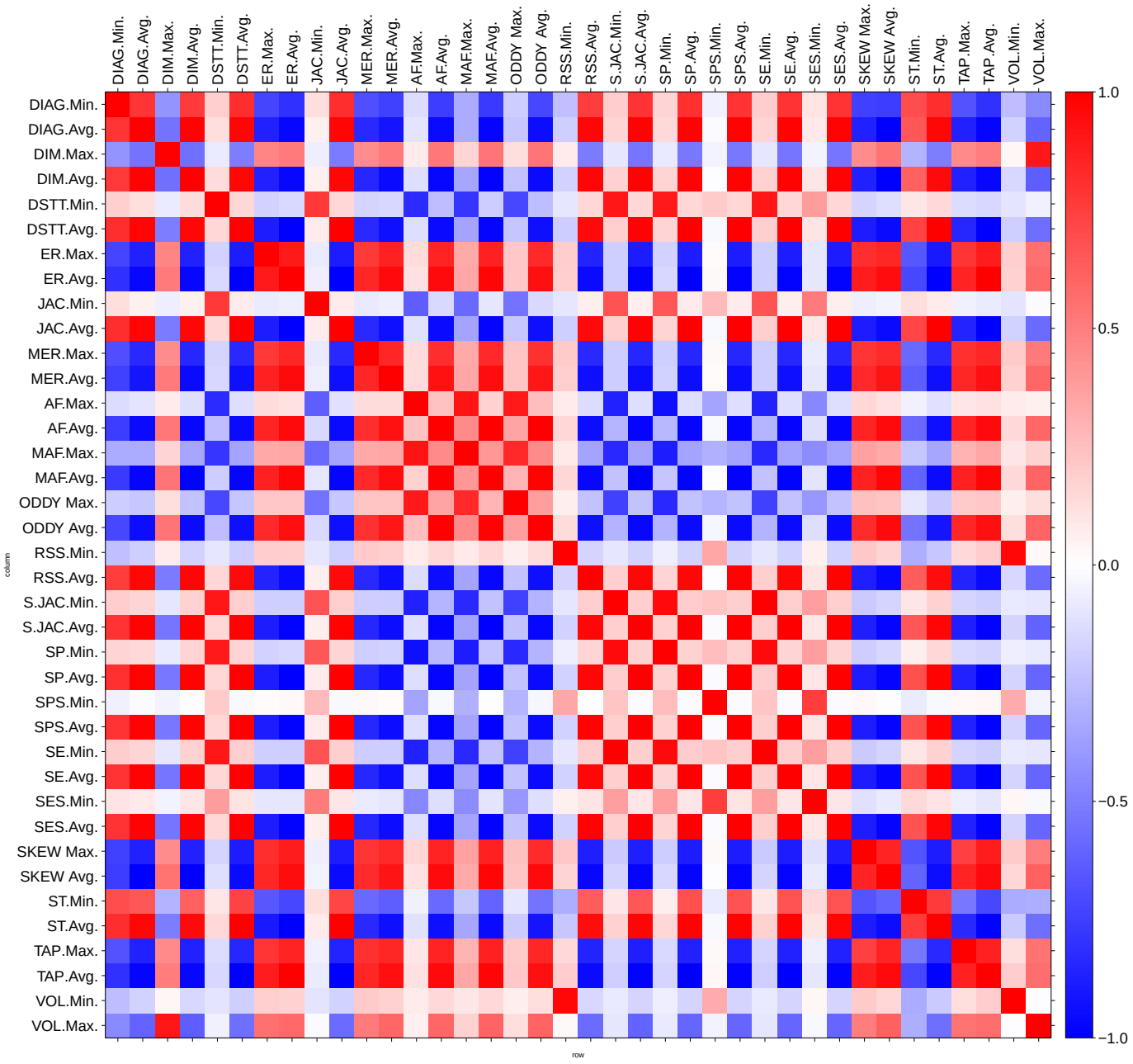

Fig. 44: The correlation matrix of the 38 metrics for the rockerarm model.

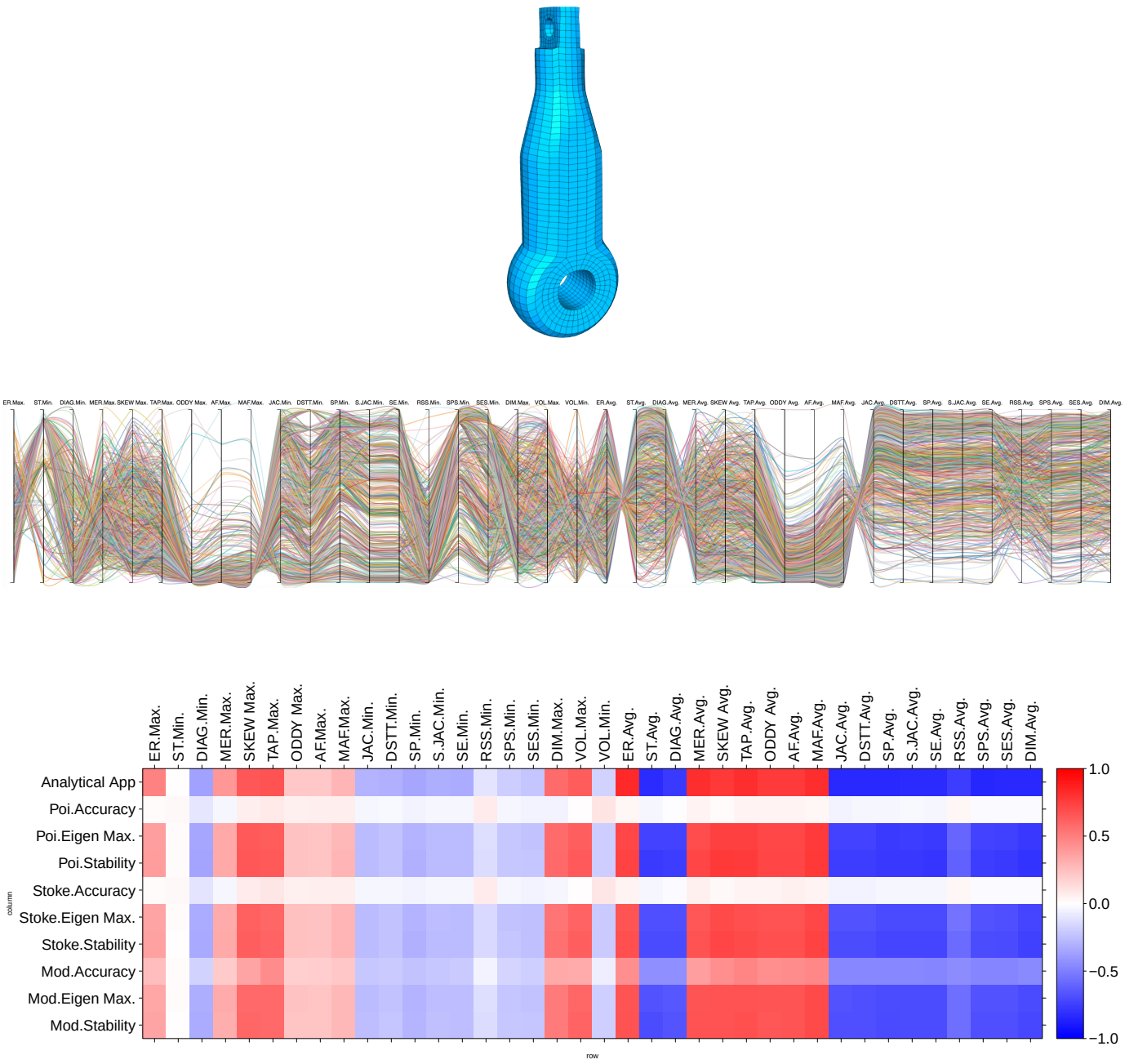

Fig. 45: The rod model (top), the parallel coordinate visualization of the sampled meshes (786 in total) in the metric space (middle), and the correlation matrix of the 38 metrics versus the Accuracy, Stability, and the difference of the solved maximal eigenvalue from the ground-truth (i.e., Max.Eigen) for the three simulations and the analytical application (bottom).

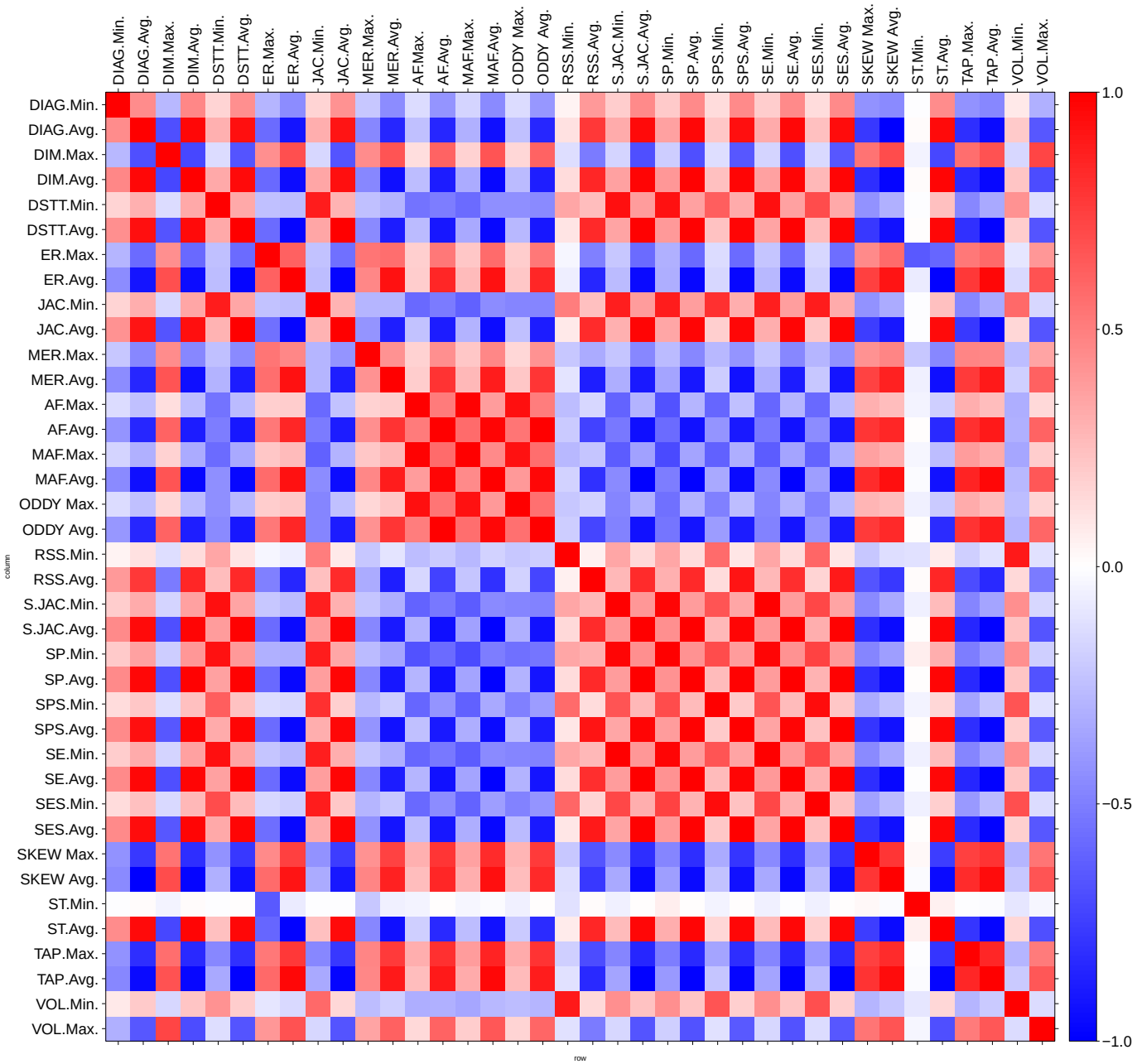

Fig. 46: The correlation matrix of the 38 metrics for the rod model.